ACIBADEM MEHMET ALI AYDINLAR UNIVERSITY
INSTITUTE OF HEALTH SCIENCES

MOLECULAR INSIGHTS INTO THE SURFACE OF THERMOALKALOPHILIC LIPASES TOWARD UNRAVELING THE INTERPLAY BETWEEN THERMOSTABILITY AND OLIGOMERIZATION

İLAYDA AMANOĞLU

MASTER THESIS

DEPARTMENT OF BIOSTATISTICS AND BIOINFORMATICS

SUPERVISOR
Prof. Emel Timuçin

ISTANBUL-2023

ACIBADEM MEHMET ALI AYDINLAR UNIVERSITY
INSTITUTE OF HEALTH SCIENCES

MOLECULAR INSIGHTS INTO THE SURFACE OF THERMOALKALOPHILIC LIPASES TOWARD UNRAVELING THE INTERPLAY BETWEEN THERMOSTABILITY AND OLIGOMERIZATION

İLAYDA AMANOĞLU
MASTER THESIS

DEPARTMENT OF BIOSTATISTICS AND BIOINFORMATICS

SUPERVISOR
Prof. Emel Timuçin

ISTANBUL-2023

DECLARATION

I declare that this thesis work is my own work, I had no unethical behavior at any stages from the planning to the writing of the thesis, I obtained all the information in this thesis in accordance with academic and ethical rules, I cited all the information and comments that were not obtained with this thesis work, and I provided resources in the list of references. I also declare that there was no violation of any patents and copyrights during the study and writing of this thesis.

06.07.2023

İlayda Amanoğlu

PREFACE AND ACKNOWLEDGEMENT

I would like to thank my advisor Emel Timuçin and our department head Osman Uğur Sezerman for their patience and motivation throughout my master's life and throughout this thesis. Especially, I would like to give my special thanks to my advisor Emel Timuçin, for her support throughout the thesis. Also, I would like to give my endless respect and thanks to Özgür Gül, who started me on my academic career journey. He will never be forgotten and will remain in our hearts.

I would like to thank Acibadem University R&D Laboratory for the opportunities they have provided us in the laboratory studies of this thesis. I would also like to thank TRUBA for giving us the opportunity to run the MD simulations of the thesis.

I would like to thank my colleagues in the department, Lara Naserikhojasteh and Zeynep Kavalcı, for their support in this thesis and for being a source of motivation for me. Their academic achievements and scientific approaches have inspired me. I am grateful to them for making me feel that they are always with me.

Last but not least, I would like to express my endless thanks to Ömürcan Sarıkaya, who gave me his endless love, motivated me, and give me the power I need to achieve everything in life. I would like to express my endless thanks to my mother Seher Coşkun, who listened to me with all her patience and helped me overcome my stress, to my brother Arda Amanoğlu and to my father Alpay Amanoğlu, who always supported me with whatever I needed.

TABLE OF CONTENTS

DECLARATION v

PREFACE AND ACKNOWLEDGEMENT vi

LIST OF ABBREVIATIONS AND SYMBOLS ix

LIST OF FIGURES xi

LIST OF TABLES xiv

ÖZET 1

ABSTRACT 2

1 INTRODUCTION AND AIM 3

1.1 Protein Engineering 3
1.1.1 Protein engineering techniques 4
1.1.2 Molecular dynamic simulations 5

1.2 Lipase 6

1.2.1 Lipase mechanism 7
1.2.2 Lipase selectivity 8
1.2.3 Lipase structure 8
1.2.4 Interfacial activation of lipase 10
1.2.5 Lipase in industry 11
1.2.6 Lipase family 11

1.3 BTL2 11

1.3.1 Biochemistry 11
1.3.2 Structure 12
1.3.3 Active site and catalytic cleft 13
1.3.4 Lid and zinc domain 14
1.3.5 Oligomerization 15
1.3.6 The importance of engineer lipase 17

1.4 Aim of The Thesis 18

2 BACKGROUND 19

3 MATERIALS AND METHODS 20

3.1 Computational Methods 20

3.1.1 Oligomer construction 20
3.1.2 in-silico mutagenesis 20
3.1.3 System preparation 21

3.1.4 Molecular dynamic simulations 21
3.1.5 Data analysis 22
3.2 Experimental Methods 22
3.2.1 Transformation 22
3.2.2 Lipase expression 23
3.2.3 Lipase purification 24
3.2.4 Lipase characterization 25
3.2.5 SDS-PAGE 25
3.2.6 Protein concentration, buffer exchange, and storage 25
3.2.7 Protein concentration measurement 25
3.2.8 Thermal incubation 26
3.2.9 Lipase thermostability and activity assay 27
4 RESULT 29
4.1 Computational Methods 29
4.1.1 Oligomer structures 29
4.1.2 in-silico mutagenesis 32
4.1.3 MD simulation 33
4.1.4 Lipase backbone stability analysis 34
4.1.5 Lipase backbone fluctuation analysis 35
4.2 Experimental Methods 44
4.2.1 Lipase production 44
4.2.2 Lipase thermostability and activity analysis 46
5 DISCUSSION 50
5.1 Lipase Thermostability and Activity Analysis 50
5.2 Analyses of Molecular Dynamic Simulations 51
6 CONCLUSION 54
7 REFERENCES 55
8 APPENDIX 61
9 CURRICULUM VITAE 65

LIST OF ABBREVIATIONS AND SYMBOLS

A	Alanine, Ala
Å	Angstrom
AMBER	Assisted Model Building with Energy Refinement
BTL2	*Bacillus thermocatenulatus* Lipaz
Ca^{+2}	Calcium Ion
CHARMM	Chemistry at Harvard Molecular Mechanics
Cl^{-}	Chloride Ion
DNA	Deoxyribonucleic Acid
ECEPP	Empirical Conformational Energy Program for Peptides
ES	Enzyme-substrate (ES)
FS	Femtosecond
Gly	Glycine
GROMOS	GROningen MOlecular Simulation
H	Histidine, His
His	Histidine
IPTG	Isopropyl-β -D-thiogalactopyranoside
K	Kelvin
kDa	Kilodalton
LB	Luria-Bertani
M	Molar
MD	Molecular Dynamics
mG	Milligram
mL	Milliliter
mM	Milimolar
µM	Micromolar
µS	Microsecond
Na^{+}	Sodium Ion
NAMD	Nanoscale Molecular Dynamics
nM	Nanomolar
NMR	Nuclear magnetic resonance

NPT	Isothermal–Isobaric Ensemble NS Nanoseconds
OD	Optical Density
PDB	Protein Data Bank
PME	Particle Mesh Ewald
QM	Quantum Mechanical
RDF	Radial Distribution Function
RG	Radius of Gyration
RGYR	Radius of gyration
RMSD	Root Mean Square Deviation
RMSF	Root mean square fluctuation
SDS	Sodium Dodecyl Sulfate
Ser	Serine
TAG	Triacylglycerol
TRUBA	Turkish National Science e-Infrastructure
VMD	Visual Molecular Dynamics
W	Tryptophan, Trp
Y	Tyrosine, Tyr
Zn^{+2}	Zinc Ion

LIST OF FIGURES

Figure 1. Schematic representation of the protein engineering techniques. 4
Figure 2. BTL2 crystal structures. The structure on the A is 1KU0, the monomer closed structure. The structure on the B is 2W22, monomer open structure. Blue colors are β sheets, orange colors are α helices and gray colors are loop regions. Images were obtained through VMD using PDB structures. NewCartoon was used as a representation. 9
Figure 3. BTL2 homodimer crystal structure. Images were obtained from the 1JI3 PDB structure using VMD (34). NewCartoon was used as a representation method. Blue colors are β sheets, orange colors are α helices and gray colors are loop regions. 10
Figure 4. Pairwise sequence alignment result of open and closed structure of lipase. Open structure 2W22 is monomer. Closed structure 1JI3 is homodimer. 13
Figure 5. W211, W60 and zinc binding site are shown with lid on BTL2 constructs. VMD was used to represent crystal structure. A is 1JI3 closed structure and B is 2W22 open structure. Zinc is colored in green, W211 is colored in blue, W60 is colored in red, and lid is colored in orange. 14
Figure 6. Mutations on 1JI3 are shown via VMD with the cartoon representation method. Only Chain A is shown in the crystal structure. The part shown in orange is the lid part. The green one is zinc. Blue indicates mutation sites. The W60A mutation is on the alpha helix and the W211 is on the lid. The zinc binding site is located between these two points. Y273A and Y282A mutations have been shown on beta sheets. 16
Figure 7. Cartoon representation of the 1JI3 homodimer structure via VMD. The green one represents the B chain and the gray one represents the A chain. Mutations are shown in blue, Zn^{+2} in green. Shown in orange color is the lid region. Looking at the image, it was thought that this triad is important in oligomerization and may affect thermostability and activity. 17
Figure 8. Cartoon representation of the 1JI3 homodimer structure via VMD. It is a clearer representation of where the homodimer structure joins. The green color represents the B chain and the gray color represents the A chain. Mutations are shown in blue, zinc in green. Lid region is shown in orange color. 17

Figure 9. Visual representation of PCR tubes that are used for thermostability analysis. 27
Figure 10. Standard Curve for 4-MU-caprylate and RFU (79)..... 28
Figure 11. Sequence alignments of 27 crystal structures were made and their similarities were shown as indicated in Table 1..... 29
Figure 12. Dimer structure of 1JI3 with Zn^{+2} and Ca^{+2}. Illustrated with Chimera in cartoons. Zn^{+2} is represented with orange and Ca^{+2} is represented with blue. The B chain is shown in green, and the A chain in gray..... 30
Figure 13. A: Tetramer structure of 1JI3. The B chain is shown in green, and the A chain in gray. Illustrated with Chimera in cartoons. A is tetramer with Zn^{+2} and Ca^{+2}. Zn^{+2} is represented with orange and Ca^{+2} is represented with blue. B is tetramer without Zn^{+2} and Ca^{+2}. 31
Figure 14. Octamer structure of 1JI3 with Zn^{+2} and Ca^{+2}. Illustrated with Chimera in cartoons. Zn^{+2} is represented with orange and Ca^{+2} is represented with blue. The B chain is shown in green, and the A chain in gray..... 32
Figure 15. Root mean square deviation (RMSD) analysis of dimer (A), tetramer (B), octamer (C), W211A (D), Y273A/Y282A/W211A (E) and W60A/W212A (F)..... 34
Figure 16. Root mean square fluctuation (RMSF) analysis of dimer (C). Visualization of the dimer crystal structure of before (A) and after (B) simulation by using VMD. Chains are indicated in different colors and listed in A and B. W211 region is represented with blue color, Y273 and Y282 regions are represented with green. ... 35
Figure 17. Root mean square fluctuation (RMSF) analysis of tetramer (C). Visualization of the tetramer crystal structure of before (A) and after (B) simulation by using VMD. Chains are indicated in different colors and listed in A and B. W211 region is represented with blue color, Y273 and Y282 regions are represented with green. 37
Figure 18. Root mean square fluctuation (RMSF) analysis of octamer (C). Visualization of the octamer crystal structure of before (A) and after (B) simulation by using VMD. Chains are indicated in different colors and listed in A and B. W211 region is represented with blue color, Y273 and Y282 regions are represented with green. 38

Figure 19. Root mean square fluctuation (RMSF) analysis of W211 mutant (C). Visualization of the W211A mutant crystal structure of before (A) and after (B) simulation by using VMD. Chains are indicated in different colors and listed in A and B. W211 region is represented with blue color, Y273 and Y282 regions are represented with green. 40
Figure 20. Root mean square fluctuation (RMSF) analysis of W60A/W211A (C). Visualization of the octamer crystal structure of before (A) and after (B) simulation by using VMD. Chains are indicated in different colors and listed in A and B. W211 region is represented with blue color, Y273 and Y282 regions are represented with green. 41
Figure 21. Root mean square fluctuation (RMSF) analysis of Y273A/Y282A/W211 mutant (C). Visualization of the octamer crystal structure of before (A) and after (B) simulation by using VMD. Chains are indicated in different colors and listed in A and B. W211 region is represented with blue color, Y273 and Y282 regions are represented with green color 43
Figure 22. BL21 Transformation. BTL2 wild type, W60A, W211A, W60A/W211A, Y73A, Y282A, Y73A/Y282A and Y73A/Y282A/W211A mutation clones were transformed to BL21 cells on LB Agar ampicillin plates. 44
Figure 23. E. coli Shuffle Expressions. Whole cell-fraction were used from wild-type and mutants, collected after 3 hours IPTG induction. Analyzed in 10% SDS-PAGE which is stained with Coomassie blue. 45
Figure 24. Residual activity versus temperature analysis. Relative fluorescent unit values were converted to percent activity by setting the activity at 4°C to 100%. 47
Figure 25. In the closed and open structure of BTL2, W211 in the lid region and its surroundings are shown 51

LIST OF TABLES

Table 1. Enzymes, showing 90% or more similarity to the 1KU0 closed structure, were examined and 27 crystal structures were listed (42). 12
Table 2. List of studied mutations and wild type DNA clones. 23
Table 3. Thermal incubation temperature set for all enzymes. Enzymes were incubated for 10 minutes at the indicated temperatures. 26
Table 4. System details of the BTL2 oligomer and mutated structures. 33
Table 5. Protein concentrations measured by nanodrop (A280) are referred in μM. 46
Table 6. In the results obtained after lipase thermostability and activity analysis, the temperature ranges in which the enzyme shows the highest activity are listed. 49

ÖZET

Termostabilite ve Oligomerizasyon Arasindaki Etkileşimi Çözmeye Yönelik Termoalkalofilik Lipazlarin Yüzeyine Moleküler Çikarimlar

Termoalkalofilik lipazlar olarak bilinen izole edilmiş lipaz ailesinin bir üyesi olan *Bacillus thermocatenulatus* lipaz (BTL2), sert sıcaklıklar altında çeşitli reaksiyonları katalize etme özelliğinden dolayı endüstriyel kullanım potansiyeli göstermektedir. Termoalkalofilik lipazlar endüstriyel üretim sürecinde gıda, deterjan ve ilaç gibi alanlarda oldukça yaygın olarak kullanılmaktadır. Agregasyon (kümeleşme) özelliklerini anlamak enzimin endüstriyel süreçte kullanımının iyileştirilmesine katkıda bulunabilir. Bu çalışma ile lipazın kullanım alanının genişletilmesi ve kullanım koşullarının optimum hale getirilmesi ile sektöre katkı sağlanması amaçlanmıştır. Bu tezde BTL2 kümeleşmesi modellenmiştir. Oligomerlerde, her iki ucu etkileşimde olan zincirlerin daha kararlı olduğu anlaşılmıştır. Bu da oligomer yapısı büyüdükçe kararlılığın artabileceğini göstermiştir. Ayrıca bu kümeleşmeyi etkileyebilen hidrofobik amino asitler araştırılmıştır. BTL2 enzimi üzerindeki spesifik W211A, W60A/W211A ve Y273A/Y282A/W211A mutasyonlarının oligomerizasyon, kararlılık ve aktivite üzerindeki etkilerini incelemek amacıyla termostabilite enzim tahlil deneyleri uygulanmıştır. Vahşi tip enzimde oligomerizasyona bağlı kararlılığı koruma etkisi göstermiştir ve bu etki mutantlarda kaybolmuştur. W211A mutasyonunun oligomerizasyon oluşumunu engellediği ve enzimlerin ısı kararlılığını azalttığı gözlemlenmiştir. Y273A/Y282A/W211A mutasyonu ise oligomerizasyonu ve ısı kararlılığını korumaya devam etmiştir. Tüm bu mutantlar ve oligomer sistemler için MD simülasyonları yapılmıştır. Simülasyon ve laboratuvar deney sonuçları birbirini doğrulamıştır. Bağlanma bölgesindeki W211A mutasyonu yapıyı bozarken Y273A/Y282A/W211A mutasyonu yapıyı korunmuştur.

Anahtar Sözcükler: BTL2, Termoalkalofilik lipazlar, MD simülasyon, Oligomerizasyon.

ABSTRACT

Molecular Insights Into The Surface Of Thermoalkalophilic Lipases Toward Unraveling The Interplay Between Thermostability And Oligomerization

Bacillus thermocatenulatus lipase (BTL2), a member of the isolated lipase family known as thermoalkalophilic lipases, shows potential for industrial use due to its ability to catalyze various reactions under harsh temperatures. Thermoalkalophilic lipases are widely used in the industrial production process in areas such as food, detergent, and medicine. Understanding the aggregation properties can contribute improving the use of enzyme in the industrial process. With this study, it is aimed to make a great contribution to the sector by expanding the usage area of lipase and optimizing the usage conditions. BTL2 oligomerization was modeled in this thesis. In oligomers, chains that interact at both ends were found to be more stable. This indicates that the stability could increase when the size of oligomers increased. In addition, hydrophobic amino acids that may affect this aggregation were investigated. Thermostability enzyme assay experiments were applied to investigate the effects of W211A, W60A/W211A and Y273A/Y282A /W211A mutations on the oligomer BTL2 enzyme on stability, and activity. It showed the effect of maintaining stability due to oligomerization in wild-type enzyme, and this effect was lost in mutants. It has been observed that the W211A mutation inhibits the formation of oligomerization and decreases the thermostability of enzymes. The Y273A/Y282A/W211A mutation continued to preserve oligomerization and thermostability. MD simulations were performed for all these mutants and oligomer systems. Simulation and laboratory test results contribute to each other. The W211A mutation in the binding site disrupted the structure, while the Y273A/Y282A/W211A mutation preserved the structure.

Keywords: Thermoalkalophilic lipases, BTL2, MD Simulations, Oligomerization.

1 INTRODUCTION AND AIM

1.1 Protein Engineering

Proteins are linear heteropolymers, that can contain 20 different amino acids. They are involved in almost all the developmental, regulatory, and sensory processes in biological systems. Proteins can change in the evolutionary process, as well as through mutation or recombinant DNA technology (1). Protein engineering is a field that combines concepts such as genetics, biochemistry, computational biology, and molecular biology. This field aims to increase the functionality, efficiency, stability, thermostability, specificity or binding of proteins (2).

There are many applications for enzymes. Environmental friendliness, substrate specificity and high catalytic activity are some of the main reasons for this. Enzymes have seen a lot of applications recently, especially in food, detergent, and health industries. Enzymes must be used effectively and with high stability in industrial production. However, insufficient use of enzymes in this process is an important issue. Proteins are denatured at high temperatures and exhibit poor stability and activity. It will also be affected by other factor such as efficiency. Because of these, the use of enzymes in industrial processes poses several difficulties. The discipline of protein engineering is trying to solve these problems.

Protein engineering is the process of producing new proteins with useful technological and scientific properties or modifying their structure and function to improve proteins. They can be formed by protein engineering techniques such as mutagenesis, rational design, molecular dynamics and directed evolution (3). There are numerous uses for protein engineering in biotechnology, food industry, cleaning industry and medicine. For example, it can be used to develop new treatments with improved therapeutic efficacy or fewer side effects, or to produce enzymes with improved catalytic activity for use in industrial processes (4). While these studies provide a great benefit in terms of health in medicine, they have a great importance in terms of reducing costs in the industrial field. Proteins are composed of amino acid

sequences, and these sequences determine the function of the protein, such as characteristics, catalytic activity, and expression level. Protein engineering identifies the required sequence and adjusts it to enhance or reconstruct function (5).

1.1.1 Protein engineering techniques

The term "protein engineering" refers to a wide range of methods used to modify, produce, or improve proteins with desired properties. Protein engineering consists of three main methods; mutagenesis, directed evolution and rational design (6).

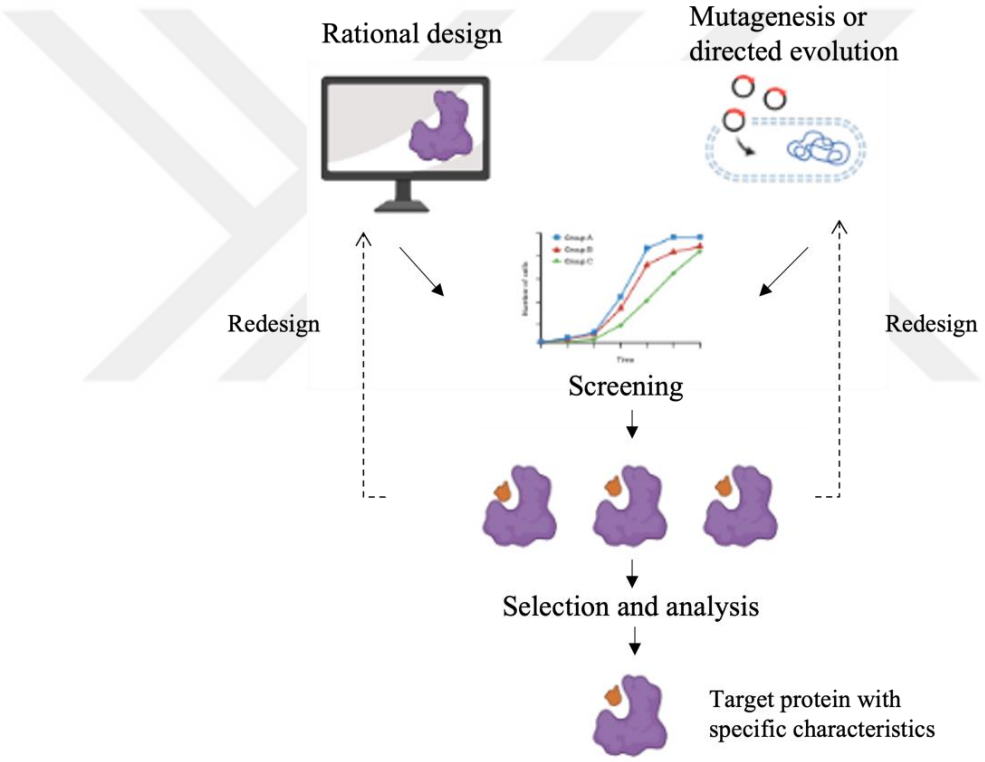

Figure 1. Schematic representation of the protein engineering techniques.

Mutagenesis, one of the protein engineering techniques, involves making random mutations to the protein sequence for the desired properties. Mutagenesis has advantageous than other methods because it is fast and has a lower error proneness. Both directed evolution and rational design methods for protein engineering are generally based on mutagenesis. Recently, literature has indicated that this method has

been used to improve the most important properties of the enzyme, such as thermostability (7). Directed evolution, is the application of selective pressure to the protein through repeated mutations and selection iterations to produce variants with traits, that are desired to be improved. In the past, directed evolution relied on a two-step process, first creating molecular diversity through random mutagenesis and in vitro recombination, followed by improvements in the desired trait by high-throughput screening or selection. Library design has been further distorted and constrained by biases in experimental techniques and degeneration of the genetic code (4).

The other method, rational design is a method for calculating the effect of changes in the protein sequence for the desired feature on the protein structure. This method incorporates small amounts of amino acid variations based on 3D information, using preselected target regions and information about the sequence, structure and function of proteins and computational predictive algorithms for protein engineering (8). Techniques such as machine learning, QM calculations and MD simulations are used in sequence and structure-based designs. It is aimed to examine the effects of amino acid changes on protein stability, such as substrate specificity, substrate activity, and developing new functions. With this method, the changes made in the amino acid sequence on the function and structure of the protein are understood in detail (7). In this thesis, the rational design technique was used in protein interface studies.

1.1.2 Molecular dynamic simulations

Protein engineering uses the powerful computational method of molecular dynamics (MD) simulation to investigate the behavior of proteins at the atomic level. MD, a powerful computer technique, creates configurations of a system by integrating classical mechanics to calculate the time dependence of the system. It is possible to investigate protein dynamics, conformational changes, and interactions between proteins and ligands using MD simulations that model the movements and interactions of atoms in a protein system over time. MD simulations are used for these purposes, refining X-ray and NMR structures, providing useful information on the creation of new proteins with desired properties, protein stability, linking between structure and

function. MD simulations provide important information about the behavior of the protein. Certain tools and calculations are needed to make analyzes of MD simulations (9).

MD facilitates the acquisition of information about the movements of biological molecules, which are often difficult to observe. It enables the investigation of folding, stability, conformational changes, and dynamic biological processes. Longer simulation timeframes and larger systems require more processing power. However, as computer speeds and parallel computing algorithms improved, as the accuracy of computer modeling techniques. Many force fields corresponding to the potential energy of the static protein structure can be used in MD simulations (10). Force fields such as ECEPP, NAMD, Hagler's, Herman's, AMBER, Allinger's, MM2 and CHARMM (11), and GROMOS are used to describe the energy of the protein. These force fields are used to construct a wire model of a protein, and various formulations are used to calculate the bound (such as rotations) and unbound (such as van der Waals and electrostatic) potential energies of the protein. The combined potential and kinetic energies of the thermal motions of atoms form, the total energy of a protein molecule at any temperature above absolute zero Philips (12).

In this thesis, NAMD, which is the most preferred software package, was used. CHARMM-GUI input generator system, which is developed by Dr. Im's research team at Lehigh University, Bethlehem, was used to generate NAMD force fields (13).

1.2 Lipase

Lipases, which are enzymes that catalyze the hydrolysis of ester bonds in lipids, are quite common in nature. Lipases are produced by animals, plants, and microorganisms. In nature, it has an effect on digestion, lipid metabolism and many biological functions. It was first discovered by Eijkmann in the 1900s, noticing that some bacteria secrete lipase out of the cell to break down lipids. The lipase has a hydrophobic core in the center and a hydrophilic structure surrounding the core. The catalytic triple amino acids (histidine, aspartate, and serine) required for the activity of

enzyme are located at the junction of these two regions. Lipases (EC 3.1.1.3, triacylglycerol lipase), one of the most crowded enzyme classes, belong to hydrolases and are enzymes on which many protein engineering studies have been applied (14). Numerous methods are used in the investigation of lipases, including protein engineering techniques, X-ray crystallography and biochemical testing. The structure and properties of lipases can be altered by protein engineering to produce variations in properties that are superior or novel to the desired properties. X-ray crystallography is used to understand the three-dimensional structure and mode of action at the atomic level of lipases. The activity and selectivity of lipases are evaluated by means of biochemical tests under various conditions. In studies conducted for many years, the structures, selectivity, and mechanism of lipases have been determined, which paves the way for further studies (15).

1.2.1 Lipase mechanism

Although lipases can catalyze a wide variety of reactions and their reaction mechanisms are different. These are versatile reactions such as hydrolysis, esterification, and transesterification. All lipases share three residues that carry out the catalytic mechanism. These are serine, histidine, and aspartate/glutamate. Two residues (histidine and aspartate/glutamate) need to be sequenced to lower the pKa of the serine hydroxyl and allow serine to perform a nucleophilic attack on the ester bond. The acyl donor substrate interacts with the active site of the lipase to produce the enzyme-substrate (ES) complex or Michaelis complex (16).

In the catalytic triad, histidine acts as an essential base and activates the hydroxyl group of serine. Serine is prepared to carry out a nucleophilic attack on the carbonyl carbon of the substrate to form the first tetrahedral intermediate. The main chain amide groups of the two residues stabilize the gap created by the negative charge on the oxyanion, while the aspartate-glutamate of the catalytic triad stabilizes the positive charge on histidine. Following the acyl enzyme intermediate, a second tetrahedral intermediate is produced, corresponding to the highest energy barrier of the reaction, such as the first intermediate. The non-deacylated version of the enzyme prepared for

the next cycle and hydrolysis of the second substrate, an acid, is also produced by the breakdown of this intermediate. During this deacylation process, proton is transmitted via serine oxygen from the substrate to the histidine (17).

1.2.2 Lipase selectivity

Lipases usually have three types of selectivity towards TAGs (triacylglycerols) which are stereo-selectivity, regio-selectivity, and substrate-selectivity (18). Stereoselectivity means that one stereoisomer (enantiomer or diastereomer) selects the other stereoisomer. This situation differs according to the type of lipase and substrate (19). Regio selectivity depends on the position of the ester bonds in the TAG. Some lipases are called as nonspecific enzymes that catalyze the reactions of all hydroxyl groups. Lipases, specific to 1.3 only, catalyze the primary hydroxyl group reactions of TAG. *Bacillus thermocatenulatus* (BTL2) is an example of these lipases. It is the enzyme in which the most common studies of microbial lipases are carried out. (20). Substrate selectivity is the selectivity of lipases with respect to the acyl groups and chain length of the substrate. Lipases may be of particular interest to chains of certain lengths and fatty acids. In many studies, it was determined that lipases mostly preferred the chain length range of C6 (medium) and C16 (long) (21,22). *Bacillus thermocatenulatus* is one of the exception lipases that prefer the C4 chain (23).

1.2.3 Lipase structure

The 3D structure of more than a hundred lipase is determined by X -ray crystallography and published. In 1990, the first lipase structure was published by Brady (24). When all these structures are examined, many features of lipase structure can be explained in general.

- Since all lipases belong to the α-β hydrolase fold, their structures consist of a β sheet and α helices. The highly conserved pentapeptide sequence Gly-X-Ser-X-Gly has the active nucleophilic serine residue in a hairpin spin between a strand and helix. The conserved pentapeptide sequence Gly-X-Ser-X-Gly

found around the active site of many other lipases is absent in some lipases, such as from *Candida Antarctic* lipase B (Calb) (25).

- The catalytic triad of the amino acids histidine, serine and aspartic acid/glutamic acid composes the active site of lipases. Lipases and proteases have active sites that are physically different but chemically identical. Since lipase serine hydroxyl group is positioned differently than serine proteases, the catalytic triad has inverted stereochemistry (26).
- Lipases have a lid structure consisting of amphilic helical that covers their active sites. The size and composition of this lid varies among lipases. For example, Lipase B from *C. antarctica* has a lid that is very small and does not cover the active site, while 20% of *Bacillus thermocatenulatus* lipase consists of a lid consisting of two α helices (27).
- Lipases have a unique catalytic cleft, and they can have different geometric structures. Stereoselectivity in lipases depends on the interaction of this cleft with the substrate and it is critical to understanding stereoselectivity (28).

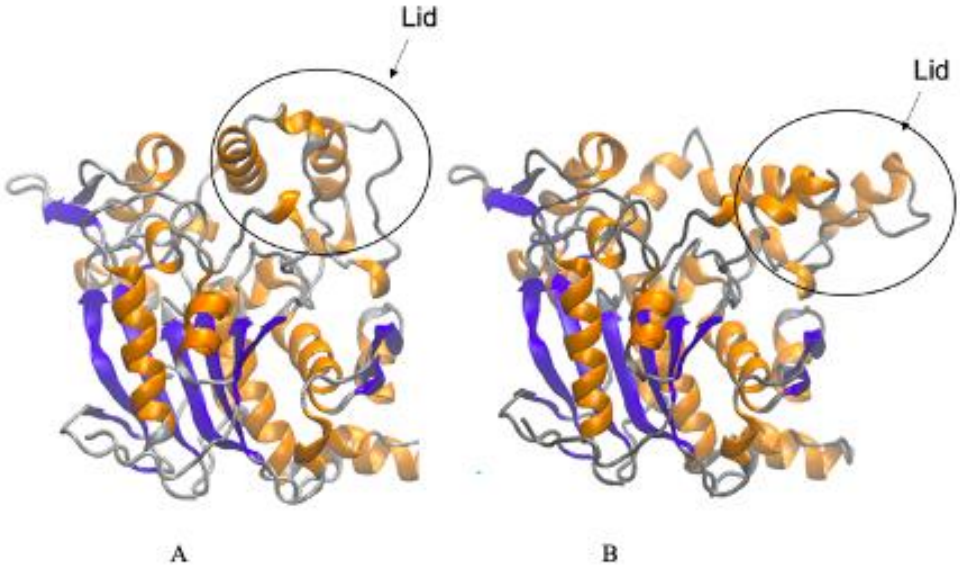

Figure 2. BTL2 crystal structures. The structure on the A is 1KU0, the monomer closed structure. The structure on the B is 2W22, monomer open structure. Blue colors are β sheets, orange colors are α helices and gray colors are loop regions. Images were obtained through VMD using PDB structures. NewCartoon was used as a representation.

1.2.4 Interfacial activation of lipase

The phenomenon called lipase interface activation is low on monomeric substrates, whereas its activity increases considerably when the aggregate substrate is formed. The presence of a collapsible lid consisting of α helices in the active region of the lipase showed that, accessing to the active region that cannot be accessed. In the presence of a hydrophobic surface, that lid opens and the lipase changes from the closed form to the opened form (29). Researches have shown that the interface activation phenomenon occurs with hydrophobic proteins and other open lipase molecules (30). The hydrogen bonds between the tryptophan is important for the catalytic function and conformation of the lid (26).

Many structures of lipase, both open and closed, have been crystallized in the literature (31). In this thesis, the closed lipase "1JI3" PDB (Protein Data Bank) (32) structure was used for simulations. The reason for the use of this structure is that when lipases are high aggregates, they are in the form of a closed structure. In order to simulate and examine the form of BTL2 in nature, the closed structure was studied.

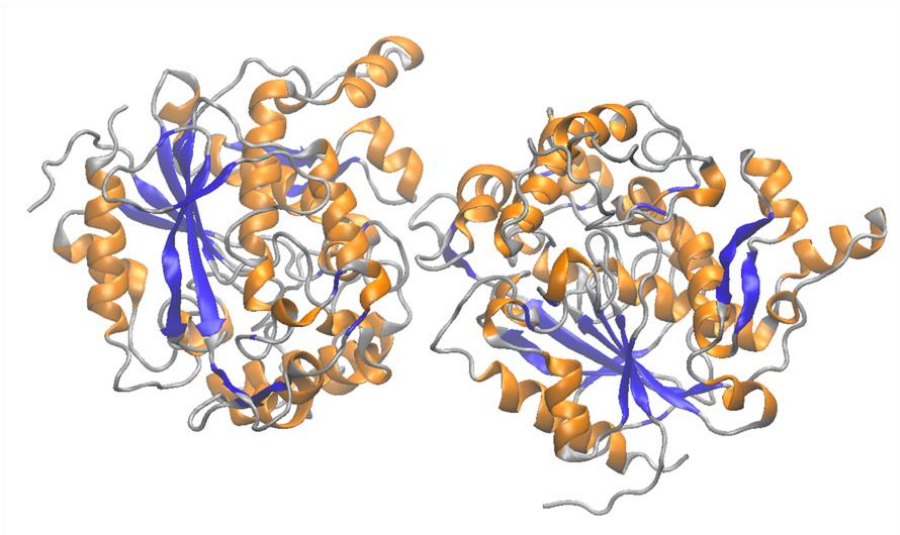

Figure 3. BTL2 homodimer crystal structure. Images were obtained from the 1JI3 PDB structure using VMD (34). NewCartoon was used as a representation method. Blue colors are β sheets, orange colors are α helices and gray colors are loop regions.

1.2.5 Lipase in industry

Lipases are generally used in the industry, in the production of detergents, production of biodiesel from vegetable and animal oils, as well as in the food industry as flavor enhancers and fat reducers. In addition to all these sectors, they are used in industry for many products such as pharmaceutical intermediates, polymers, and aroma compounds (33). Giving detailed examples of the industrial use of lipases: In the pulp industry, pitch is separated by enzymatic separation and lipase is used for this process (34). It serves to bypass the grinding part in the textile industry and reduces toxic exposure. Lipases are produced enantioselectivity in the pharmaceutical industry to reduce toxicity and costs (35). Since BTL2 is a thermostable lipase, it has great importance in the industry as it is tolerant to the difficulties encountered in industrial production processes (36).

1.2.6 Lipase family

Bacterial lipases have been defined as eight lipase families based on their catalytic serine-containing motifs. Five of them have the pentamer G-X-S-X-G, and three have the pentamer A-X-S-X-G. Those with the pentamer A-X-S-X-G are members of lipase 1.5 family. These lipases show high sequence similarities, structural similarities, and common biochemical features (37). They are resistant to high temperatures and high pH, as they are generally produced by thermoalkophilic bacteria. Also, the lipase 1.5 family has a zinc binding site compared to other lipases (38). Because of all these features, the lipase 1.5 family has been the focus of enzyme engineering.

1.3 BTL2

1.3.1 Biochemistry

BTL2 is a lipase consisting of 388 residues, a molecular weight of 43 kDa, and a fragment code of 1167 bp (39). BTL2 shows selectivity towards C4 and C8 (short and medium) chains and exhibits low activity on long chains such as C10. Like other

lipases, it catalyzes the sn-1/3 acyl chain in triglycerides (40). It has been stated that BTL2 can remain stable up to 8-9 pH and 60-70°C (41). In this study, it was expected that the thermostability of wild-type BTL2 would decrease significantly after 60°C and would lose its activity at 70°C.

1.3.2 Structure

Table 1. Enzymes, showing 90% or more similarity to the 1KU0 closed structure, were examined and 27 crystal structures were listed (42).

PDB ID	Uniprot ID	Species	Oligomeric State	Biological Assembly	Resolution
1KU0	Q66015	Geobacillus stearothermophilus	Monomer	2	2.00 Å
6A12	Q8L1V2	Geobacillus thermoleovorans	Monomer	1	2.15 Å
2W22	Q59260	Geobacillus thermocatenulatus	Monomer	1	2.00 Å
5CE5	Q59260	Geobacillus thermocatenulatus	Monomer	1	2.00 Å
1JI3	Q9L6D3	Geobacillus stearothermophilus	Homo 2-mer	1	2.20 Å
4FKB	Q5U780	Bacillus sp. 42	Homo 2-mer	1	1.22 Å
5XPX	A0A0K0PTR1	Pseudomonas sp. A3(2015c)	Homo 2-mer	1	2.77 Å
4FDM	Q5I4I3	Bacillus sp. L2	Monomer	1	1.60 Å
2DSN	Q842J9	Geobacillus zalihae	Monomer	2	1.50 Å
3UMJ	Q842J9	Geobacillus zalihae	Monomer	2	2.10 Å
2Z5G	*Q842J9*	Geobacillus zalihae	Monomer	2	1.80 Å
3AUK	B9ZZP0	Geobacillus sp. SBS-4S	Monomer	1	1.66 Å
4X71	Q93A71	Geobacillus stearothermophilus T6	Monomer	1	2.00 Å
4X6U	Q93A71	Geobacillus stearothermophilus	Monomer	1	2.20 Å
6FZ7	Q93A71	Geobacillus stearothermophilus	Monomer	1	1.74 Å
6FZ1	Q93A71	Geobacillus stearothermophilus	Monomer	1	2.20 Å
4X7B	Q93A71	Geobacillus stearothermophilus T6	Monomer	1	2.40 Å
6FZA	Q93A71	Geobacillus stearothermophilus	Monomer	1	1.75 Å
7BUK	Q842J9	Geobacillus zalihae	Monomer	2	2.64 Å
6FZ8	Q93A71	Geobacillus stearothermophilus	Monomer	1	2.20 Å
6FZ9	Q93A71	Geobacillus stearothermophilus	Monomer	1	1.25 Å
6FZC	Q93A71	Geobacillus stearothermophilus	Monomer	1	2.70 Å
4FMP	Q93A71	Geobacillus stearothermophilus	Monomer	2	2.30 Å
6S3G	Q93A71	Geobacillus stearothermophilus	Monomer	1	1.90 Å
4X85	Q93A71	Geobacillus stearothermophilus T6	Monomer	1	2.19 Å
6FZD	Q93A71	Geobacillus stearothermophilus	Monomer	1	1.80 Å
6S3V	Q93A71	Geobacillus stearothermophilus	Monomer	1	2.00 Å

BTL2 is divided into open and closed structure (43). In this thesis, the closed and homodimer structure of BTL2 was used. It has the same α-β hydrolase folding region as most microbial lipases. The structure has seven hydrophobic β-sheet chains surrounded by α helices (44).

In the structures whose PDB IDs are given in Table 1, and their oligomeric states appear as monomers, the number of those with biological assembly two is high and they are crystallographic contacts. This indicates that the interface is in crystal contact or in solution contact.

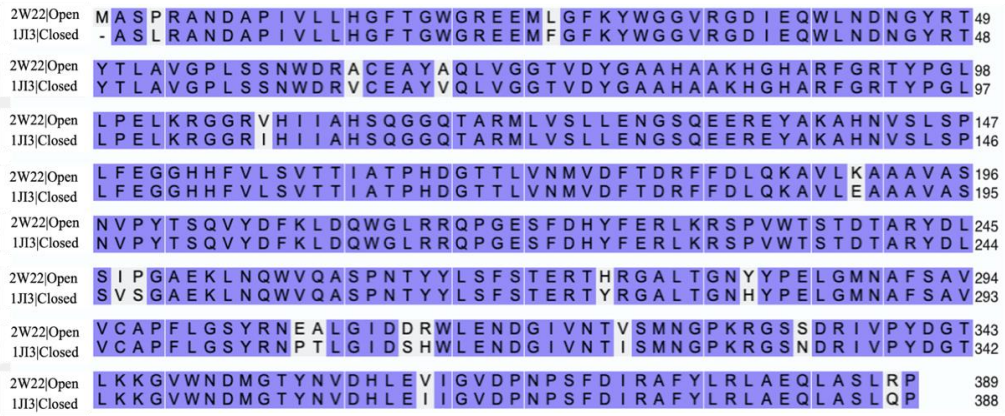

Figure 4. Pairwise sequence alignment result of open and closed structure of lipase. Open structure 2W22 is monomer. Closed structure 1JI3 is homodimer.

1.3.3 Active site and catalytic cleft

The active site and catalytic cleft of BTL2 is oval shape, with inner space dimensions of 18x25 Å2 and a depth of 14 Å. The catalytic cleft consists of about 60 amino acids that folded into two α helices (25). These amino acids are very critical for the lipase structure. It was especially important to work with W211 in this thesis, since it is thought that tryptophan amino acids in the lid of thermoalkalophilic lipases will have an effect on thermostability. A total of four binding pockets were identified in this cleft. Serine, which has an important role in balancing catalytic attacks, is also found in the motif of A-X-S-X-G (43).

1.3.4 Lid and zinc domain

The movable structure at the entrance of the catalytic cleft is called the lid. As a result of the interaction of the substrate with the lid helices, the lid opens, and this is caused by interface activation. The closed C-terminals move 20 Å away from the cleft. In the closed structure, two α helices form the lid. The first α helix split in two to fit the catalytic series to the substrate, while the other helps to widen the cleft width (41). The Zn^{+2} domain is commonly found in the lipase 1.5 family. It is hypothesized that this Zn^{+2} domain in BTL2 contributes to the enhancement of thermostability (45). As seen in the Figure 5, the W211 region is located on lid. Opposite this region is the W60 region. In the middle of the W211 and W60 regions, the zinc metal binding site is embedded.

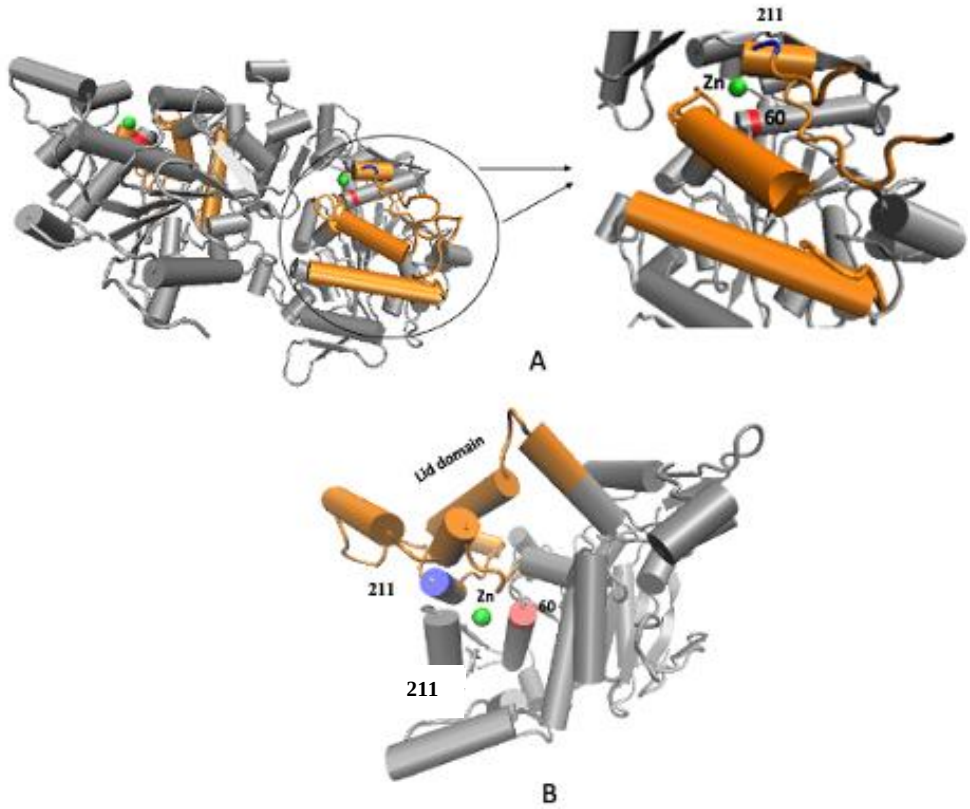

Figure 5. W211, W60 and zinc binding site are shown with lid on BTL2 constructs. VMD was used to represent crystal structure. A is 1JI3 closed structure and B is 2W22 open structure. Zinc is colored in green, W211 is colored in blue, W60 is colored in red, and lid is colored in orange.

1.3.5 Oligomerization

The term "neurodegenerative diseases" is a disorder defined by the degeneration and death of nerve cells in the brain and/or spinal cord. These disorders cause a persistent deterioration in cognitive, motor and/or behavioral functions (46). Neurodegenerative diseases are a major problem for a large population around the world. Protein aggregation are typical cellular and molecular pathways in neurodegenerative illnesses such as Alzheimer's disease, Parkinson's disease, Amyotrophic lateral sclerosis, Huntington's disease, and Prion diseases (47). It has great importance to understand the formation of aggregation in detail for offering solutions to these diseases. Protein aggregation is a key reason of many neurodegenerative disorders and plays an important role in their development. Proteins can misfold or associated abnormally under certain conditions, resulting of protein aggregation. Depending on the condition, these aggregates can take the shape of amyloid plaques, neurofibrillary tangles, or inclusion bodies. Although the mechanism leading to protein aggregation in neurodegenerative diseases has not been fully determined, but can be listed such as misfolded proteins, disruption of the natural protein clearance mechanism and seeding (48). BTL2 is an aggregation prone enzyme. Due to the intermolecular interaction of proteins during aggregation, thermal denaturation is delayed as the concentration increases. In this way, it is thought that the aggregation of thermoalkalophilic lipases serves to increase thermostability (49). The effect of aggregation on thermostability has been discussed by Ruo et al., but no definite conclusion has been reached (50).

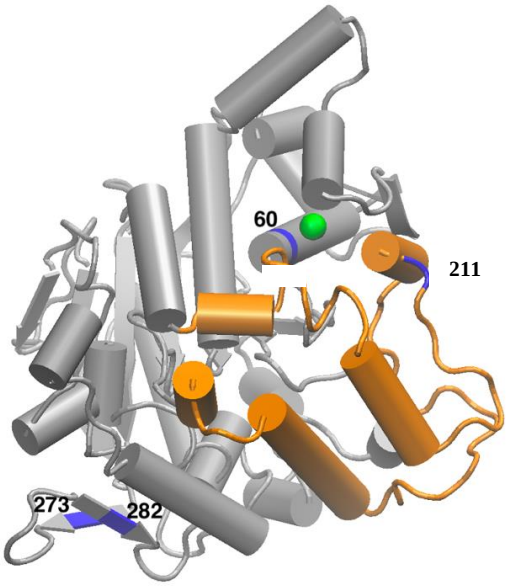

Figure 6. Mutations on 1JI3 are shown via VMD with the cartoon representation method. Only Chain A is shown in the crystal structure. The part shown in orange is the lid part. The green one is zinc. Blue indicates mutation sites. The W60A mutation is on the alpha helix and the W211 is on the lid. The zinc binding site is located between these two points. Y273A and Y282A mutations have been shown on beta sheets.

At high temperatures, the intermolecular forces of attraction loosen and the BTL2 aggregates begin to separate. Conversely, at low temperatures, interactions become more frequent on aggregates for oligomerization (51,52). Based on these interactions, it comes to mind that the relationship between aggregation and temperature should be investigated. Interactions occurring on hydrophobic amino acids play an important role (25,53). Aggregates of thermoalkalophilic lipases may not dissolve at low temperatures, whereas they can dissolve with increasing energy at high temperatures (54).

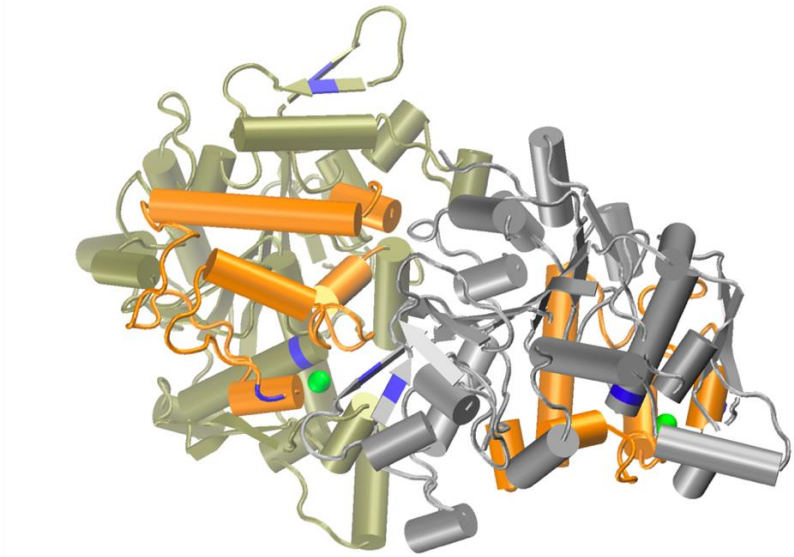

Figure 7. Cartoon representation of the 1JI3 homodimer structure via VMD. The green one represents the B chain and the gray one represents the A chain. Mutations are shown in blue, Zn^{+2} in green. Shown in orange color is the lid region. Looking at the image, it was thought that this triad is important in oligomerization and may affect thermostability and activity.

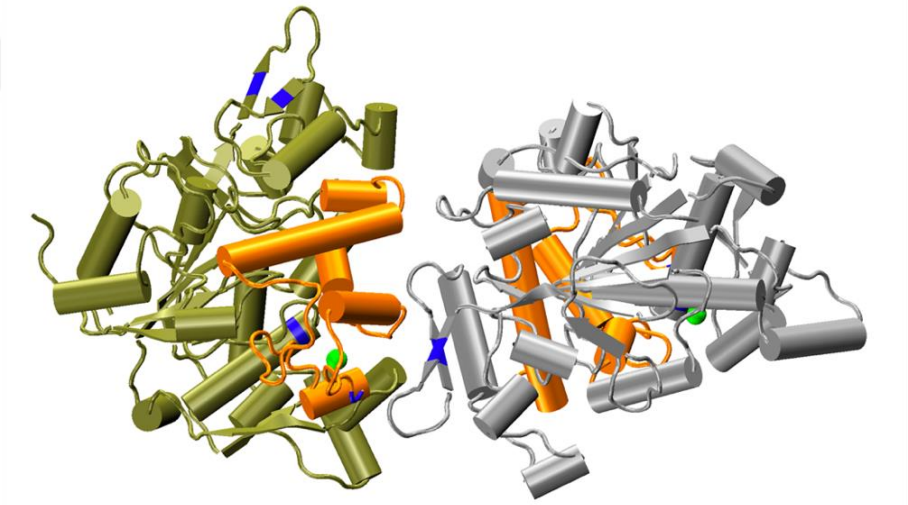

Figure 8. Cartoon representation of the 1JI3 homodimer structure via VMD. It is a clearer representation of where the homodimer structure joins. The green color represents the B chain and the gray color represents the A chain. Mutations are shown in blue, zinc in green. Lid region is shown in orange color.

1.3.6 The importance of engineer lipase

Lipases have numerous application in the industrial production process (34). Improving the process in these uses is the domain of protein engineering. One of the

most popular topics in protein engineering is lipases, due to the wide area of use of lipases. They address many issues, such as changing the substrate selectivity of the enzyme or increasing its stability. One of the most important problems encountered in industrial process is caused by high temperatures. To provide a solution to this situation, protein engineering is also closely concerned with the thermostability of lipases (55).

Since lipases are thermostable, they are highly preferred in industrial applications (56). In addition, they are aggregation prone enzymes and being aggregation prone causes a decrease in enzyme solubility (57). Protein engineering techniques are important for lipases to increase enzyme solubility, understand and modify aggregation properties, and this thesis has benefited from the field of protein engineering.

1.4 Aim of The Thesis

The study in this thesis includes modeling the oligomer structures of BTL2 and understand the aggregation mechanism. Also, it is aimed to investigate of hydrophobic amino acids that can affect oligomerization/aggregation in thermoalkalophilic lipases. The subject is to examine the effects of specific mutations W211A, W60A/W211A, and Y273A/Y282A /W211A on the BTL2 enzyme for oligomerization, stability, and activity. It is aimed to understand the stability of the enzyme by examining the BTL2 oligomer structures both wild-type and with its mutant. Eliminating the conditions where thermostability can negatively affect the industrial process will enable production areas such as food, detergent, and pharmaceuticals for an easy and low-cost production process. In addition, by understanding the aggregation mechanism, it is aimed to offer a solution to the diseases caused by aggregation. Investigating the relationship between BTL2 thermostability and oligomerization, which is the main goal of this study, is thought to provide important developments for the industry and medicine.

2 BACKGROUND

Enzymes have a wide range of uses due to environmental friendliness, high catalytic activity, and substrate specificity. Giving an example of usage areas, they have been highly preferred in fields such as health, food, hygiene, and industrial production in recent years (4). Like any substance, enzymes should be used with high efficiency and high stability. However, the use of enzymes can cause some problems in this respect, and it limits their use. At high temperature, proteins are denatured, showing low stability and low activity (58). There are also other factors that will affect activity, such as aggregation. For these reasons, various protein engineering methods are used to overcome the difficulty of using enzymes in industrial processes (26).

The use of enzyme is highly preferred in the industry as it reduces the cost and increases the efficiency. In addition, their ability to catalyze the reaction in organic and aqueous environments makes them preferable. Lipases are fully degradable and renewable enzymes. Lipases prefer naturally occurring oils as substrates and have a wide variety of substrates (59). Microbial lipases have extracellular structures, so they can be produced and isolated in high concentration. This provides great convenience in the industrial production process. Microbial lipases exhibit a more stable attitude at high temperatures and organic solvents than others. They also have broad substrate selectivity and do not require cofactors (60). The reason why enzymes are important in the industrial process is that they are efficient and selective. They follow the thermodynamic rules required in chemical catalysis processes and are important for specific product synthesis. In addition, since enzymes are environmentally friendly, they reduce waste and save energy in the production process (61).

3 MATERIALS AND METHODS

3.1 Computational Methods

3.1.1 Oligomer construction

To understand the effects of BTL2 oligomerization and mutations on oligomers in terms of thermostability, activity and solubility, oligomers were created, and mutations were applied to these structures. Chimera (62) application was used for the formation of oligomers. For computational studies, the oligomeric state of the 27 crystal structures listed in Table 1, were examined and a selection was made from among homo-dimer structures. The reason for choosing homo-dimer is that lipases are in closed form due to their tendency to being high aggregates. 1JI3 PDB structure was used as BTL2 lipase for oligomer formation. The reason for this is that the homo-dimer structure showing the nearest similarity to the closed structure 1KU0 PDB structure is 1JI3. In Chimera, match maker was used with structure comparison. At this stage, after 3 homo-dimer structures were loaded to form tetramers, the A chain of one structure was sequentially fetch to the B chain of the other structure. Then, other unmatched chains were checked according to their colors on the model panel. After the structures will be deleted are determined, they were selected and deleted. At the end of the structure, a tetramer containing 2 A and 2 B chains were formed. The same processes were applied in octamer structures, respectively. A total of 7 homo-dimer structures for the octamer were loaded and the same procedures were applied. The water around the protein was deleted from the created oligomer PDB files. The water was removed to prevent any problems that may occur in the MD simulation, only the necessary ions Ca^{+2}, and Zn^{+2} were kept in the crystal structures.

3.1.2 *in-silico* mutagenesis

Mutations were generated on the tetramer to investigate the simulations with mutations. The reason for using tetramer that it is aimed to work on a structure where the difference can be seen without increasing the size of the system which could

increase the computational cost. The tetramer structures generated without ligand (Zn^{+2} and Ca^{+2}). Non-ligand constructs were constructed for W211A, W60A-W211A and Y273A/Y282A/W211A mutations. Mutations were introduced within the four chains of the tetramer. In silico mutagenesis was applied with using CHARMM-GUI. Mutations were made for all chains of the tetramer from the mutation insertion part in the CHARMM-GUI (13).

3.1.3 System preparation

The 5G1X waters in the PDB structure were cleaned and they were loaded into the system from the solution builder section of the CHARMM-GUI (13). The chains and ligands to be used were determined and selected. Mutations were made at this stage, for systems from the PDB manipulation option. The structures were placed in the center of the rectangular water box with an enter edge distance of 10.0 Angstrom. Ion additions were applied to balance the net charge in the protein and to approach physiological conditions. In this thesis, systems were neutralized by adding a minimum concentration of $Na^{+}Cl^{-}$ into the water box. Grid information for PME FFT has been selected to be automatically generated by the system. CHARMM36 force field and NAMD molecular dynamics algorithm was used to prepare systems. The system was equilibrated with NVT (63). Following all these procedures, NPT was used on the systems with a 373K Langevin temperature and 1 atm Langevin pressure (64). Periodic boundary conditions were used in all dimensions with a time step of 2 femtoseconds.

3.1.4 Molecular dynamic simulations

For MD simulation, dimer, tetramer, and octamer were simulated. The mutations listed on the tetramer BTL2 were applied. These mutations were studied without Zn^{+2}-Ca^{+2} metals. In the systems, energy minimization and relaxation were performed with multiple steps repetitively. 303K was used for the equilibration steps and 373K was used for the production steps. In the simulation, it was simulated using NAMD molecular dynamics algorithm. The steps implemented here have been applied to

increase the stability of the oligomer simulations. The systems, operated at constant pressure (1 atm) and at the above-mentioned temperatures. Constant temperature (373K) and pressure (1 atm) were used in all production simulations.

3.1.5 Data analysis

The simulations were also structurally analyzed for multidimensional root mean square deviation (RMSD), and root mean square fluctuation (RMSF). All the obtained trajectory analyzes were made by VMD (65).

The numerical measure of the difference between two constructs (a target construct and a reference construct) is RMSD. Large changes in protein structure relative to the starting point can be detected using RMSD (66). The focus point is on how structures and the elements that compose them change over time with respect to their initial state. RMSF analysis was performed to understand the time dependent movements of the structure. RMSF is the measurement of the average displacement of atoms with respect to the reference structure (67).

3.2 Experimental Methods

3.2.1 Transformation

In previous studies, cloning was done to generate mutations. A 1,167-bp DNA fragment corresponding to the BTL2 and the DNA of the mature lipase clone (pPICZα A-BTL2) were used for cloning. Primers for forward (F BTL2 LIC: 5-TACTTCCAATCCAATGAA GCGGCATCCCCACGCG -3 and for reverse (R BTL2 LIC: 5- TTATCCACTTCCAATGAA AGGCCGCAAACTCGCCAA -3). The listed mutations in Table 2. were obtained using overlap extension PCR. Mutant fragments were cloned into the pMCSG-7 backbone.

Table 2. List of studied mutations and wild type DNA clones.

Clones List	
BTL2	**W60A/ W211A**
W211A	**Y273A/Y282A**
W60A	**Y273A/Y282A/W211A**
Y273A	**Y282A**

Protein production usually consists of basic steps such as transformation, expression, purification, and characterization after DNA cloning. *E coli* is very important for recombinant DNA technology because the expression system is built on it and there is a lot of information in the literature for *E coli*. In this study, *E coli* was used for protein expression (58). Transformation via chemical transformation into *E. coli* BL21 component cells (DE3) were performed to obtain mutant clones by chemical transformation (68). For each wild type BTL2, W60A, W211A, W60A/W211A, Y273A, Y282A, Y273A/Y282A and Y273A/Y282A/W211A mutant clones, transformation procedure was performed for all. Ligation product and BL21 cells were put into eppendorfs on ice for each. The mixtures were kept on ice for 25 minutes. Then, cells were placed into the incubator at 42℃ for 1 minute for heat shock. LB was added to tubes and incubated at 37℃ for 45 minutes by shaking. Centrifuge them 7500 rpm for 1 minute. Supernatants were discarded. Cells were plated into LB agar plates that contains 100 µg/ml ampicillin and incubated at 37℃ overnight.

3.2.2 Lipase expression

Sample collection was applied for each mutant on the LB plate. Since collection will be done for expression, attention was giving to touch all colonies while collecting. After collecting all the colonies with the tip, they were incubated in shaker incubator (200 rpm) in LB medium with 100 µg/ml ampicillin at 37℃ and 18 hours for the lipase expression (69). The day after, the grown mutant samples were expressed in LB medium with 100 µg/ml ampicillin. Bacterial concentration was measured by

spectrophotometer with a light source of 600 nm until they reach OD_{600} (optical density) (70). When this value was reached, 1mM IPTG (isopropyl-β -D-thiogalactopyranoside) was added to the liquid LB culture and incubated for 3 hours (71). The cells were harvested by centrifugation (for 10 minutes, maximum speed on tabletop centrifuge) and pellets were frozen at -20℃ and stored at -80℃.

3.2.3 Lipase purification

Nickel-coated beads were used for the purification method of lipase mutants. Histidine binds to nickel and the BTL2 protein attaches to nickel columns. Then, when high concentration imidazole is given, nickels bind to imidazole and leave the proteins. Thus, pure proteins are eluted (72). Stored samples were lysed by using sonicator (for 5 minutes, 3 cycles). Cells whose walls were destroyed with a sonicator are centrifuged for 30 minutes at 4℃ and 4500 rpm. Thus, cell wastes precipitated, the supernatant was taken and loaded onto columns containing nickel-coated beads. Loading was done using a peristaltic pump. Before loading samples, binding buffer was passed through the columns as 5 columns volume. Concentrations of 15 mM imidazole for binding, 35 mM imidazole for washing and 200 mM imidazole for elution were used. At the washing step, the concentration of the wastes was checked using Bradford (73). This step is important to move from the washing step to the elution step. Bradford solution was used for an overall estimation of the concentration for the proteins. It was also used for the initial concentration estimation of the enzymes eluted after purification. The Bradford solution gives a bluish color when combined with the protein, and the blue color becomes darker as the concentration increases (58). In order to pass from the washing step to the elution step, it is expected that the blue color should be well lightened. The reason for this is that proteins that are not attached to nickel are washed and discarded. Then the BTL2 proteins were collected by elution. The liquid flowing through the columns was collected into clean eppendorfs. 30,000 Da filtration tubes were used to concentrate the expressed proteins. Centrifuge filter tubes were filled with protein samples. The centrifuge wall was positioned vertically with filter tubes inside and centrifuged at 10,000 rpm. Centrifugation continued until all the liquid had gone down. The remaining protein samples were subjected to the same procedure.

Purified and concentrated lipases were loaded onto sodium dodecyl polyacrylamide electrophoresis (SDS-PAGE) to test the purity and size of the lipases (74).

3.2.4 Lipase characterization

There were some methods used to determine lipase characterization. SDS-PAGE gel was a characterization experiment to determine the size of the enzyme, the Bradford assay to determine the concentration of the enzyme, the thermostability assay to determine the reaction of the enzyme at different temperatures, and the activity assays to understand how the activity of the enzyme changes under different conditions (75).

3.2.5 SDS-PAGE

To perform SDS-PAGE gel electrophoresis, the protein sample was first mixed with a loading buffer containing SDS and reducing agent (DTT). Then, samples were heated at 98°C for 10 minutes to denature the proteins and break any disulfide bonds. A 10% SDS-PAGE gel was prepared, markers and samples were loaded into the wells. Running was done in a controlled manner at 120V for 90 minutes. After electrophoresis, the separated proteins visualized by staining the gel with Coomassie blue. At this step, staining and then destaining process were performed (74).

3.2.6 Protein concentration, buffer exchange, and storage

1X TBS was added to the filter tube during protein concentration. All liquid was removed by pipetting well to the wall and transferred to a new tube. Proteins were stored at +4°C.

3.2.7 Protein concentration measurement

The concentrations of the concentrated and containing 1X TBS buffer proteins were measured with the Nanodrop. 1X TBS was used as a blank. Since working with protein, concentrations were measured with UV absorption at 280 nm (76).

3.2.8 Thermal incubation

The purified and concentrated lipases in 1X TBS were adjusted to 20 µM and 1 µM concentrations. Thermostability was tested by incubating at 8 different temperatures for 10 minutes. These temperatures are 4 ^{O}C , 25 ^{O}C, 50 ^{O}C, 55 ^{O}C, 60 ^{O}C, 65 ^{O}C, 70 ^{O}C, 75 ^{O}C. Ice was used for 4 ^{O}C, room temperature for 25 ^{O}C and a gradient program in PCR for other temperatures (in Table 3). After incubation the enzymes were used for activity assays.

Table 3. Thermal incubation temperature set for all enzymes. Enzymes were incubated for 10 minutes at the indicated temperatures.

Temperatures for Thermostability Analysis			
20 µM Concentration of enzymes		1 µM Concentration of enzymes	
On ice	4 °C	On ice	4 °C
Room Temperature	25 °C	Room Temperature	25 °C
PCR (Gradient)	50 °C	PCR (Gradient)	50 °C
PCR (Gradient)	55 °C	PCR (Gradient)	55 °C
PCR (Gradient)	60 °C	PCR (Gradient)	60 °C
PCR (Gradient)	65 °C	PCR (Gradient)	65 °C
PCR (Gradient)	70 °C	PCR (Gradient)	70 °C
PCR (Gradient)	75 °C	PCR (Gradient)	75 °C

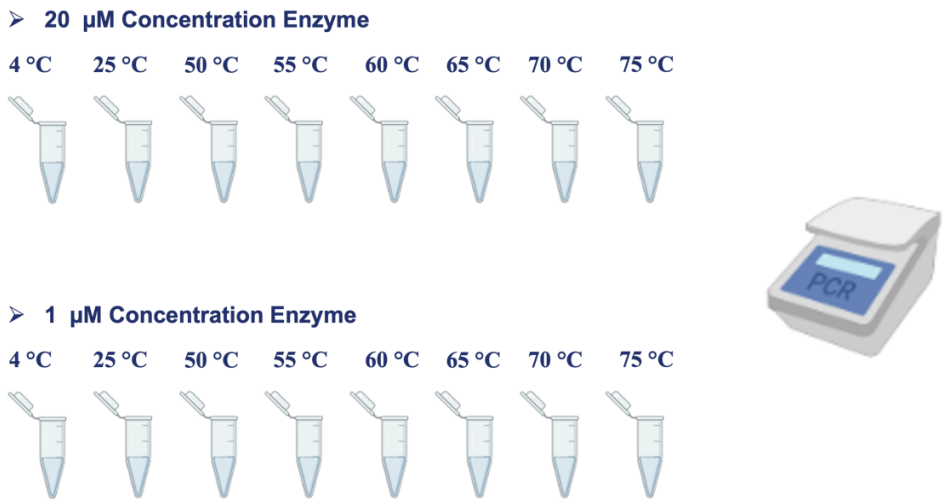

Figure 9. Visual representation of PCR tubes that are used for thermostability analysis.

3.2.9 Lipase thermostability and activity assay

There are two ways to determine lipase activities. The first is the titration assay and uses triacylglycerols (TAGs) as substrates. The second method is fluorometric assay and 4MU-caprylate based substrates are used. Concentrations of all lipase mutants were determined by Nanodrop. The effect of aggregation was also investigated at this stage by testing a high and a low concentration for the lipase activity test (75). All lipases were adjusted before the experiment so that the high concentration was 20 µM and the low concentration was 1 µM. Prior to the lipase activity test, enzyme concentrations were diluted to 1nM. The reaction mixture was prepared as 250 µM 4MU-caprylate, 100 mM Tris-Cl, 1 nM enzyme (77). Lipase activity was measured in the Thermo Varioskan instrument using a 96 well black plate for fluorescence assay, using an excitation wavelength of 365 nm and an emission wavelength of 445 nm. For all analysis, the measurements were made at every minute for 1 hour. Velocity calculation was made by looking at the kinetic calculation results. The kinetic calculation results obtained from the Varioskan were analyzed and compared. According to the linear relationship represented in Figure 10, the 4MU units are converted from the relative fluorescence unit (RFU) received from the fluorometer. Lineweaver-Burk plots were used to determine kinetic parameters (78).

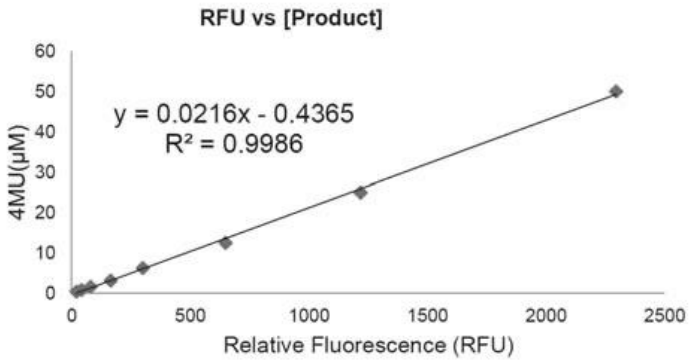

Figure 10. Standard Curve for 4-MU-caprylate and RFU (79).

4 RESULT

4.1 Computational Methods

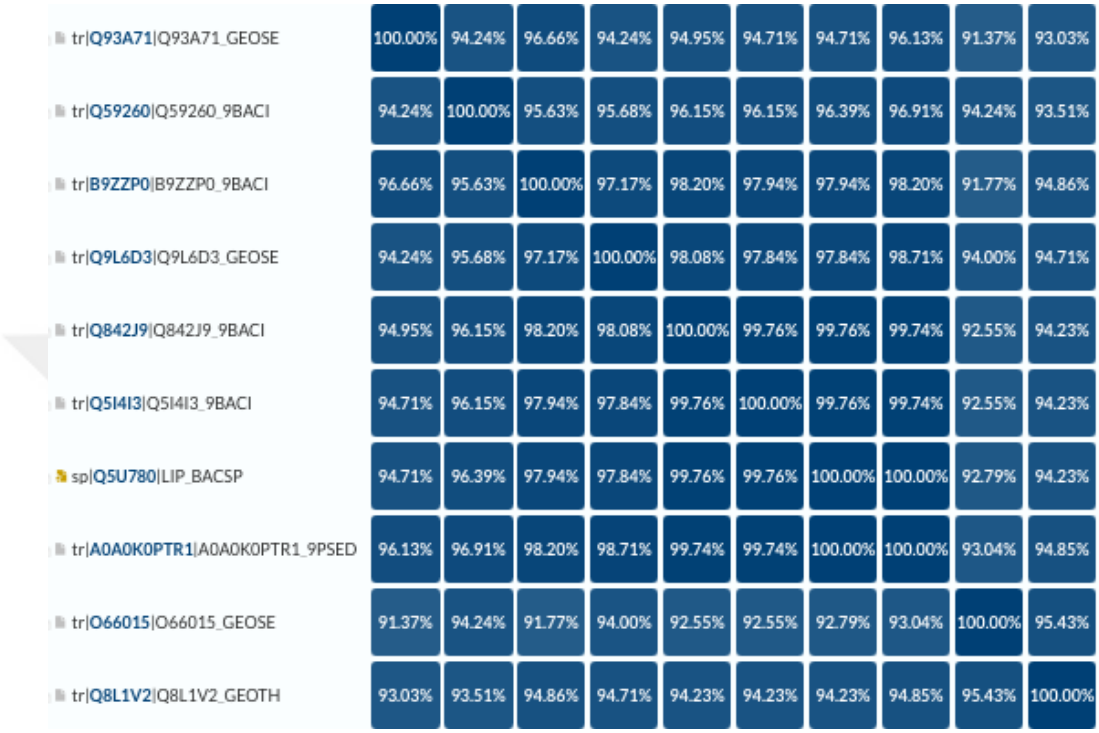

Figure 11. Sequence alignments of 27 crystal structures were made and their similarities were shown as indicated in Table 1.

4.1.1 Oligomer structures

The closed BTL2 homodimer structure was used to construct the systems. The reason for using a closed structure is that when BTL2 aggregates, it becomes a closed structure in the natural process. By using the closed structure, the proximate situation to the conditions in the natural process has been tried to be simulated. Understanding the mechanism of aggregation and effect of BTL2 oligomerization on thermostability, oligomer systems were created. Oligomer systems (dimer, tetramer, and octamer) created using Chimera are shown in the Figure 12, 13, and 14 below. The images of the systems are shown with NewCartoon using VMD. Dimer, tetramer, and octamer systems have been studied with metals. Mutant tetramers have been studied without metals. In the crystal structure images, the chain ions appear to be at the binding

interface (Zn^{+2}) as expected. The fact that it is at the binding interface supports the idea that it may be effective for activity and thermostability in oligomerization. Therefore, working with zinc metals has been an important step while creating systems in this thesis.

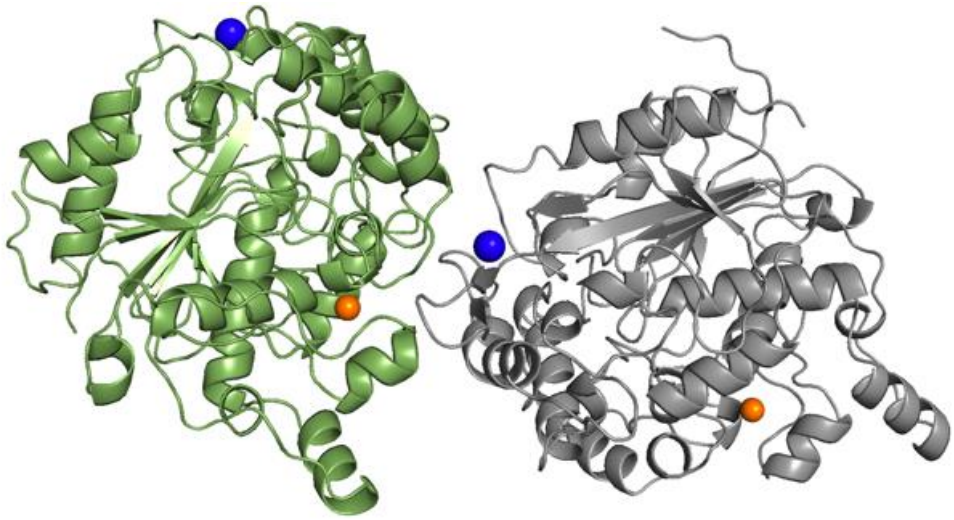

Figure 12. Dimer structure of 1JI3 with Zn^{+2} and Ca^{+2}. Illustrated with Chimera in cartoons. Zn^{+2} is represented with orange and Ca^{+2} is represented with blue. The B chain is shown in green, and the A chain in gray.

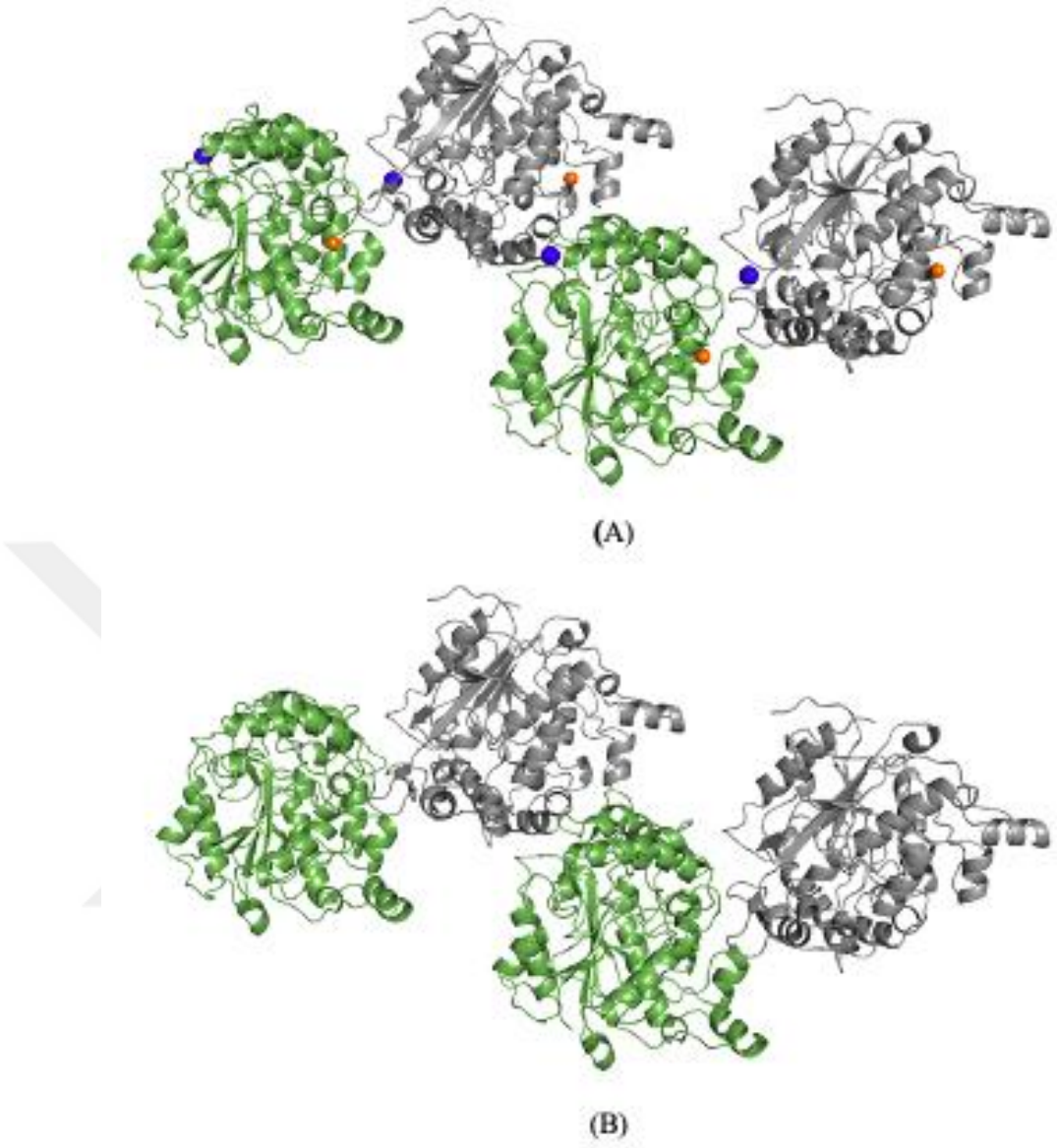

Figure 13. A: Tetramer structure of 1JI3. The B chain is shown in green, and the A chain in gray. Illustrated with Chimera in cartoons. A is tetramer with Zn^{+2} and Ca^{+2}. Zn^{+2} is represented with orange and Ca^{+2} is represented with blue. B is tetramer without Zn^{+2} and Ca^{+2}.

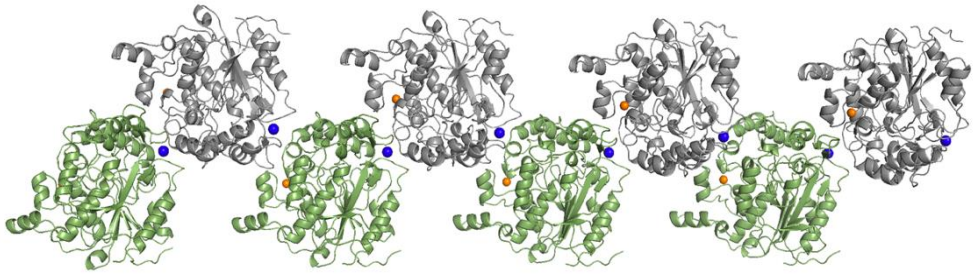

Figure 14. Octamer structure of 1JI3 with Zn^{+2} and Ca^{+2}. Illustrated with Chimera in cartoons. Zn^{+2} is represented with orange and Ca^{+2} is represented with blue. The B chain is shown in green, and the A chain in gray.

4.1.2 *in-silico* mutagenesis

Mutant structures created for MD simulations on tetramer structures via CHARMM-GUI is W211A, W60A/W211A, and Y273A/Y282A/W211A. Investigating the effect of mutations on thermostability in BTL2 aggregation, *in-silico* mutations were made on BTL2 enzymes. As seen in Figure 6, W60 and W211 are in the zinc binding site. W211 and W60 are on opposite sides of each other. W211 surrounds the zinc binding site from the lid and W60 remains in the other part of this side. In the middle of these two regions is the zinc binding region. In this thesis, W211 is an important mutation for oligomerization as it is present in both the lid and the binding interface. It was expected that the loss of tryptophan would cause a major issue, as it would affect the dielectric constant. In order to understand this, MD simulations were performed on the generated systems with mutations.

4.1.3 MD simulation

Table 4. System details of the BTL2 oligomer and mutated structures.

				Dimension (Å)		
	Atom number	**Residue**	**Water**	**x**	**y**	**z**
Dimer	175931	776	54647	152	158	168
Tetramer	535051	1552	170357	208	330	238
Octamer	425060	3104	125700	339	109	130
W211A without metal	700924	1552	225664	197	197	197
W60A/W211A without metal	700841	1552	225655	197	197	197
Y273A/Y282A/W211A without metal	700871	1552	225653	197	197	197

The systems created for MD simulation are shown in Table 4 with their details. Atom number is all atoms of the system and water is all water that systems have. Since one chain of 1JI3 has 388 amino acid (80), residue number is increasing according to chain number of oligomer. Oligomers and mutated systems were simulated in aqueous and $Na^{+}Cl^{-}$ containing environment at 373K. Oligomers were simulated as containing Zn^{+2} and Ca^{+2}. In the mutated systems, metals (Zn^{+2} and Ca^{+2}) were removed. The reason was to fully understand the effect of mutation on oligomerization of BTL2. Since the metals are at the bonding interface, we eliminated the possibility that they could increase the binding strength during oligomerization.

4.1.4 Lipase backbone stability analysis

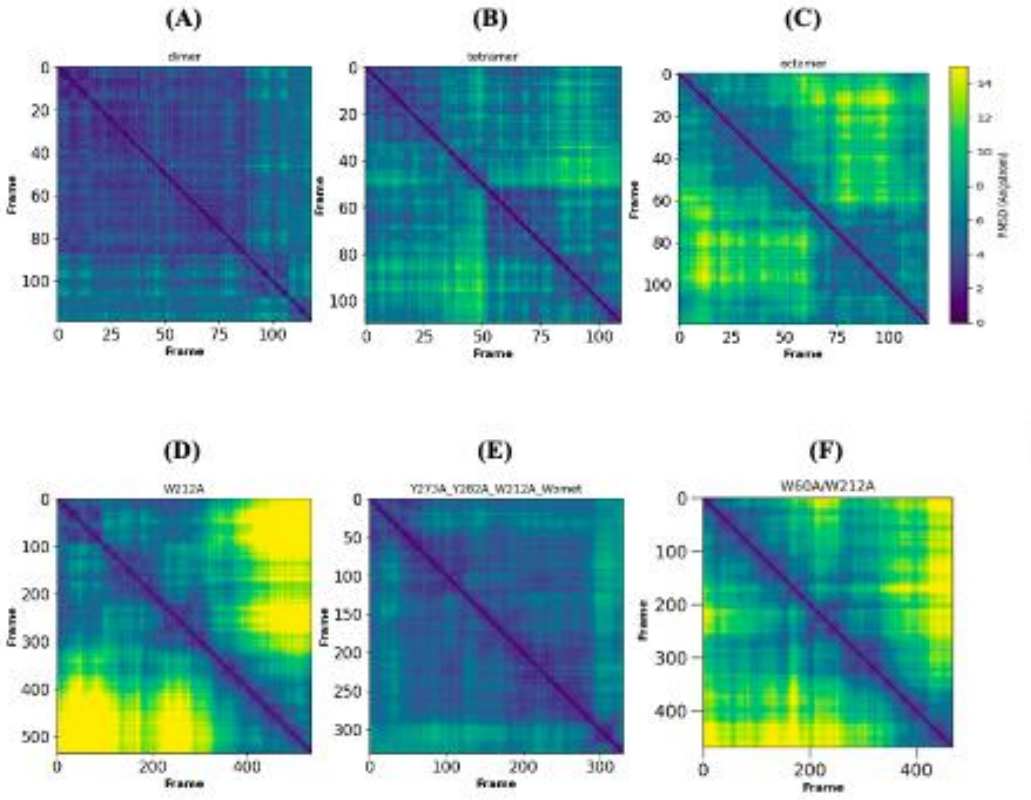

Figure 15. Root mean square deviation (RMSD) analysis of dimer (A), tetramer (B), octamer (C), W211A (D), Y273A/Y282A/W211A (E) and W60A/W212A (F).

Dimer, tetramer, and octamer systems were simulated to deeply understand how the aggregation occurs. Also, W211A, W60A/W211A and Y273A/Y282A/W211A systems were simulated. The pairwise RMSD graph of all trajectories is shown in the Figure 15. The change in color from dark blue to light yellow in the graph indicates an increased conformational change in the protein. In the simulated structures at 373K, it was observed that the displacement in the structure increases as the system grows from dimer to octamer. Considering the mutants, the W211A and W60A/W211A mutants could not store their stability, while the Y273A/Y282A/W211A mutant shows more stable profile than others.

4.1.5 Lipase backbone fluctuation analysis

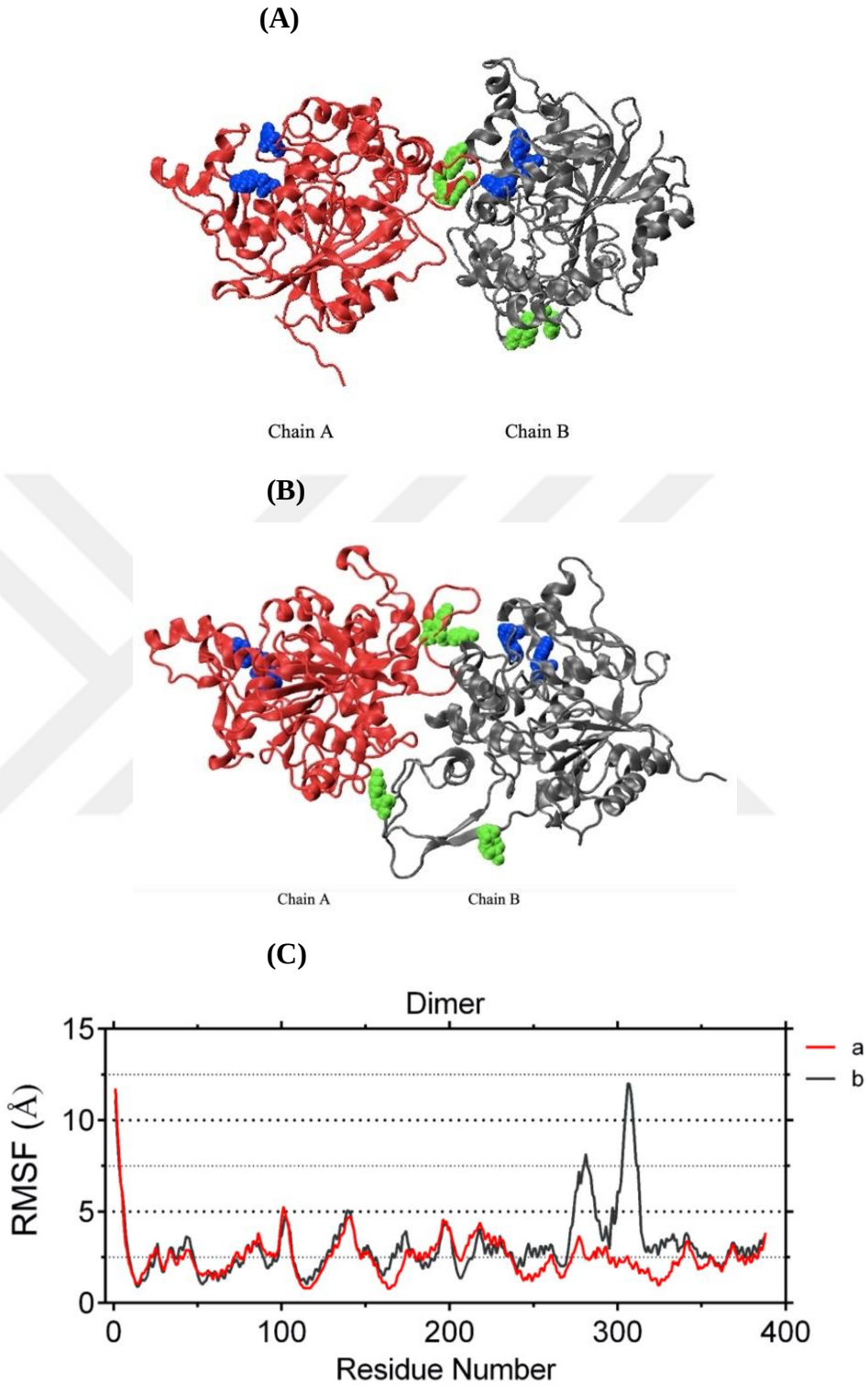

Figure 16. Root mean square fluctuation (RMSF) analysis of dimer (C). Visualization of the dimer crystal structure of before (A) and after (B) simulation by using VMD. Chains are indicated in different colors and listed in A and B. W211 region is represented with blue color, Y273 and Y282 regions are represented with green.

Looking at the dimer trajectory, it seems that Y273, Y282 and W211 form triple cluster in Figure 16. It is understood that this cluster is using for binding to other. The Y273 and Y282 residues of the A chain interacted with the W211 region of the B chain to form a dimer. The residues Y273, Y282 and W211 at the other ends of the A and B chains were exposed. When looking at the RMSF result in Figure 16C, the open part of the Y273 and Y282 regions of the B chain have quite moved and it gave a peak in the graph. Difference can be seen with the before and after trajectory pictures in Figure 16A and 16B. While this region was the most mobile part in the B chain, the 211th region of the A chain, which it is attached to Y273 and Y282 of the B chain, seems quite stable.

When the tetramer trajectory is analyzed, it is seen that the four chains (A, B, C and D) of tetramer attached to each other with the W211, Y273 and Y282 regions. In the tetramer structure, the A and C chains are outside, the B and D chains are inside. Regions in the interior remained more stable because of the strong interaction by the cluster. These regions hold each other tightly, like holding hands, with strong interaction. Looking at the RMSF graph in Figure 17, the outer B and C chains could not remain stable and were quite mobile. The A and D chains, which are attached by clusters on both sides, remained more stable and did not move like B and C chains. In Figure 17C, residues 273 and 282, which are in the region of the highest peak, appeared in the B chain. When looking at the before and after trajectory pictures (Figure 17A and 17B), this area is outside, so it is the most mobile and suitable area for interaction.

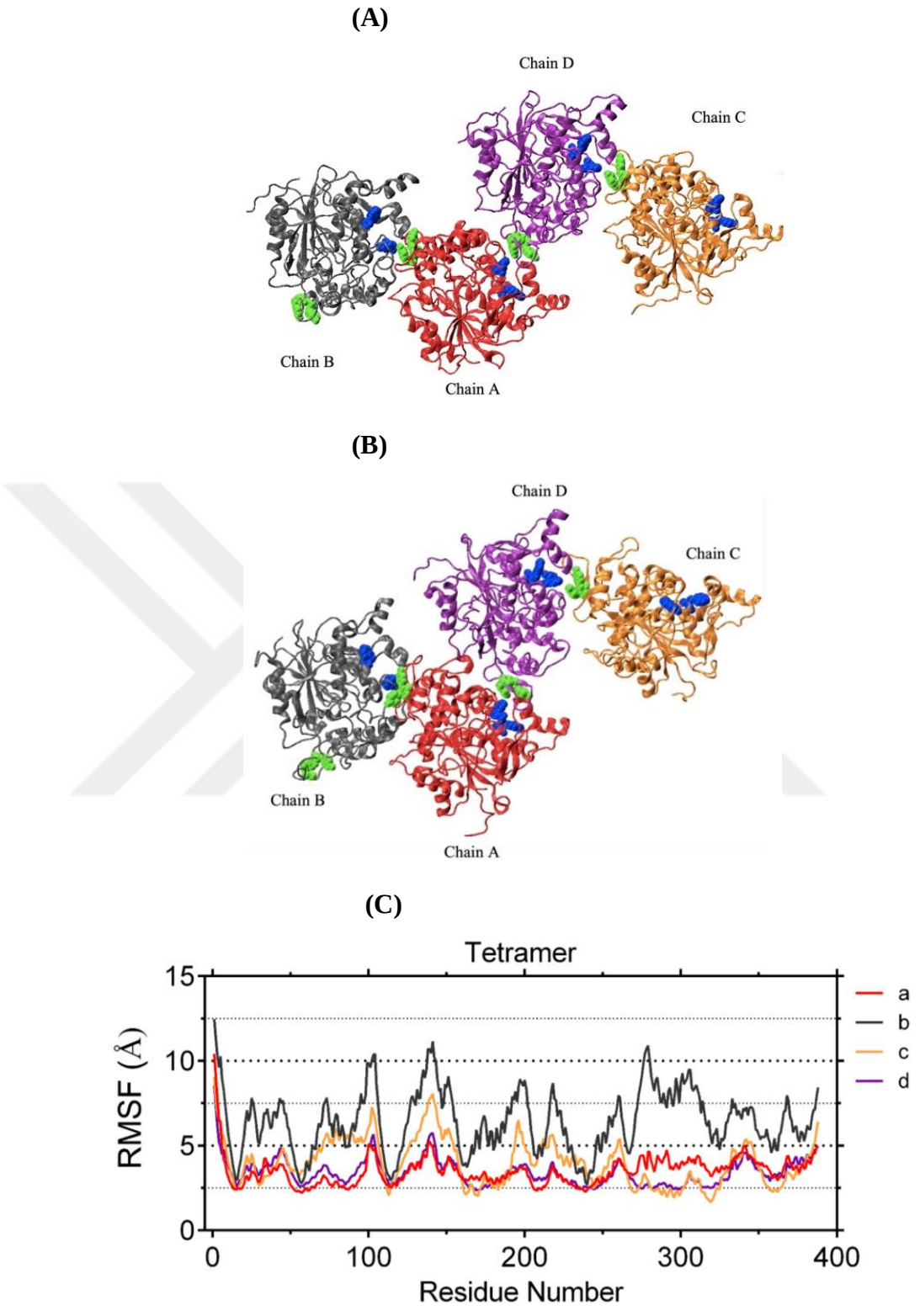

Figure 17. Root mean square fluctuation (RMSF) analysis of tetramer (C). Visualization of the tetramer crystal structure of before (A) and after (B) simulation by using VMD. Chains are indicated in different colors and listed in A and B. W211 region is represented with blue color, Y273 and Y282 regions are represented with green.

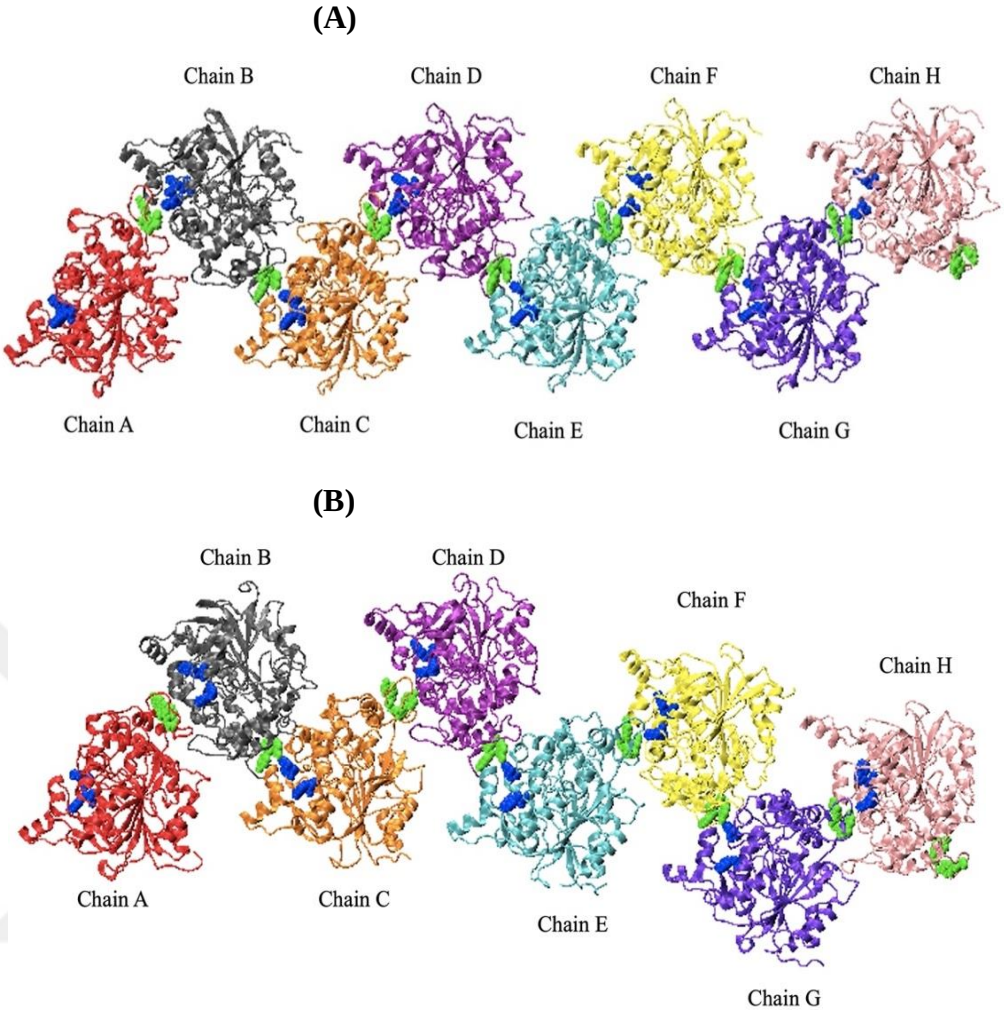

Figure 18. Root mean square fluctuation (RMSF) analysis of octamer (C). Visualization of the octamer crystal structure of before (A) and after (B) simulation by using VMD. Chains are indicated in different colors and listed in A and B. W211 region is represented with blue color, Y273 and Y282 regions are represented with green.

When the octamer trajectory is examined, it is seen that all eight chains of the octamer (A, B, C, D, E, F, G, and H) were also attached to each other by the W211, Y273 and Y282 regions. In the octamer structure, the A and H chains are outside and the other chains are inside. Due to the strong interaction of the cluster, regions in the interior remained more stable. These regions are tightly connected to each other, as holding hands in a strong interaction. Looking at the RMSF graph in Figure 18C, the outer A and H chains gave more peaks so they seem to be quite mobile. While the region that remained unattached, 211^{th} region in the A chain and the 273-282 region in the H chain was mobile. Other chains, connected in clusters on both sides and remained more stable. Looking at the before and after trajectories in Figures 18A and 18B, it is seen that the unattached chains were displaced more.

In Figure 19, it was understood that the oligomerization of the structure was impaired. To explain in more detail, in the W211A mutation made in the BTL2 tetramer as an oligomeric state, the tetramer structure was disrupted by W211A mutation. This supports the idea that W211 is on the binding interface and important for aggregation. Looking at the RMSF graph in Figure 19C, all chains of the tetramer appear to be quite mobile. Looking at the before and after trajectories in Figures 19A and 19B, it is seen that the B chain almost completely separated from the structure. Looking at the other chains of the mutant tetramer, it is seen that they moved quite more.

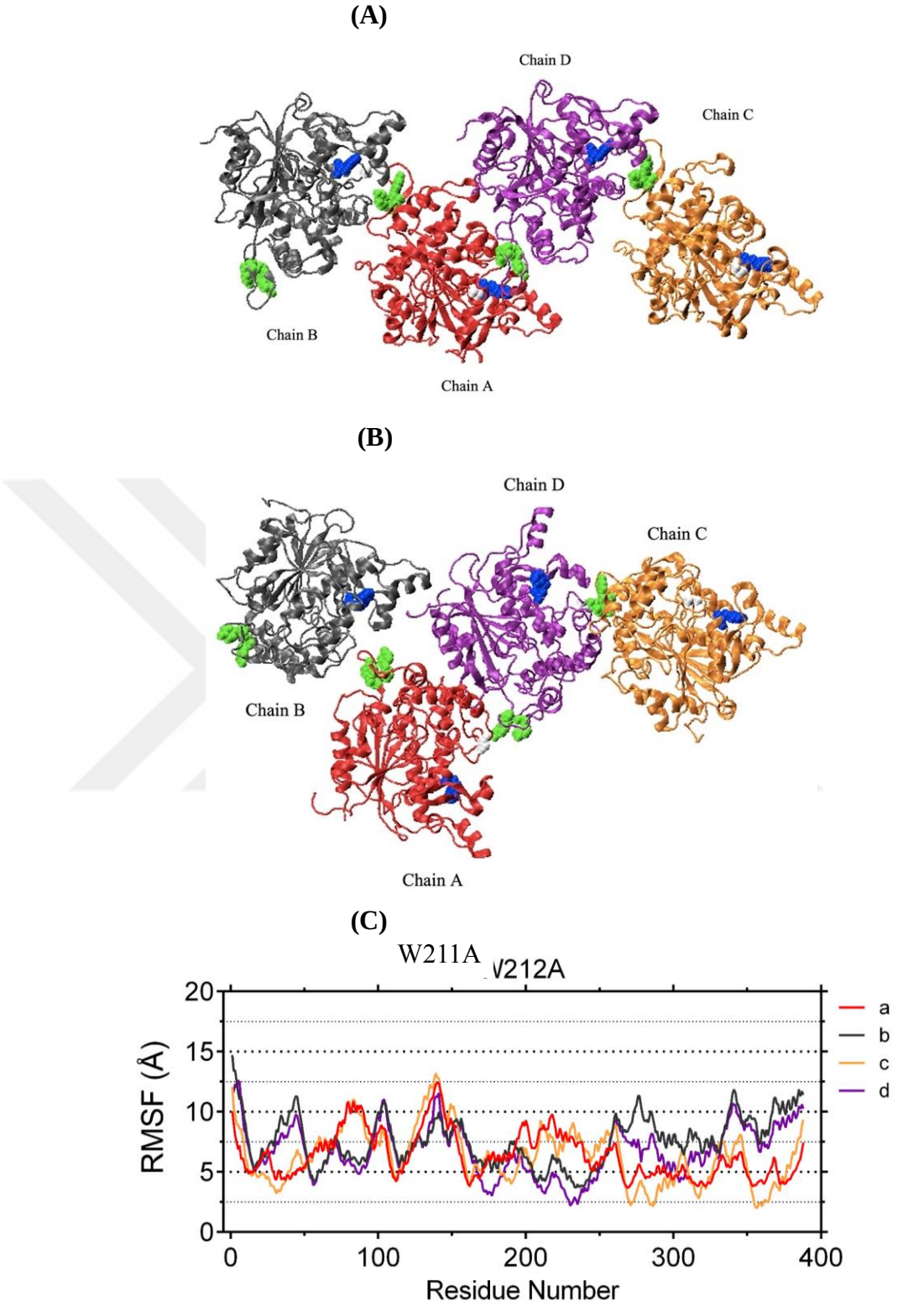

Figure 19. Root mean square fluctuation (RMSF) analysis of W211 mutant (C). Visualization of the W211A mutant crystal structure of before (A) and after (B) simulation by using VMD. Chains are indicated in different colors and listed in A and B. W211 region is represented with blue color, Y273 and Y282 regions are represented with green.

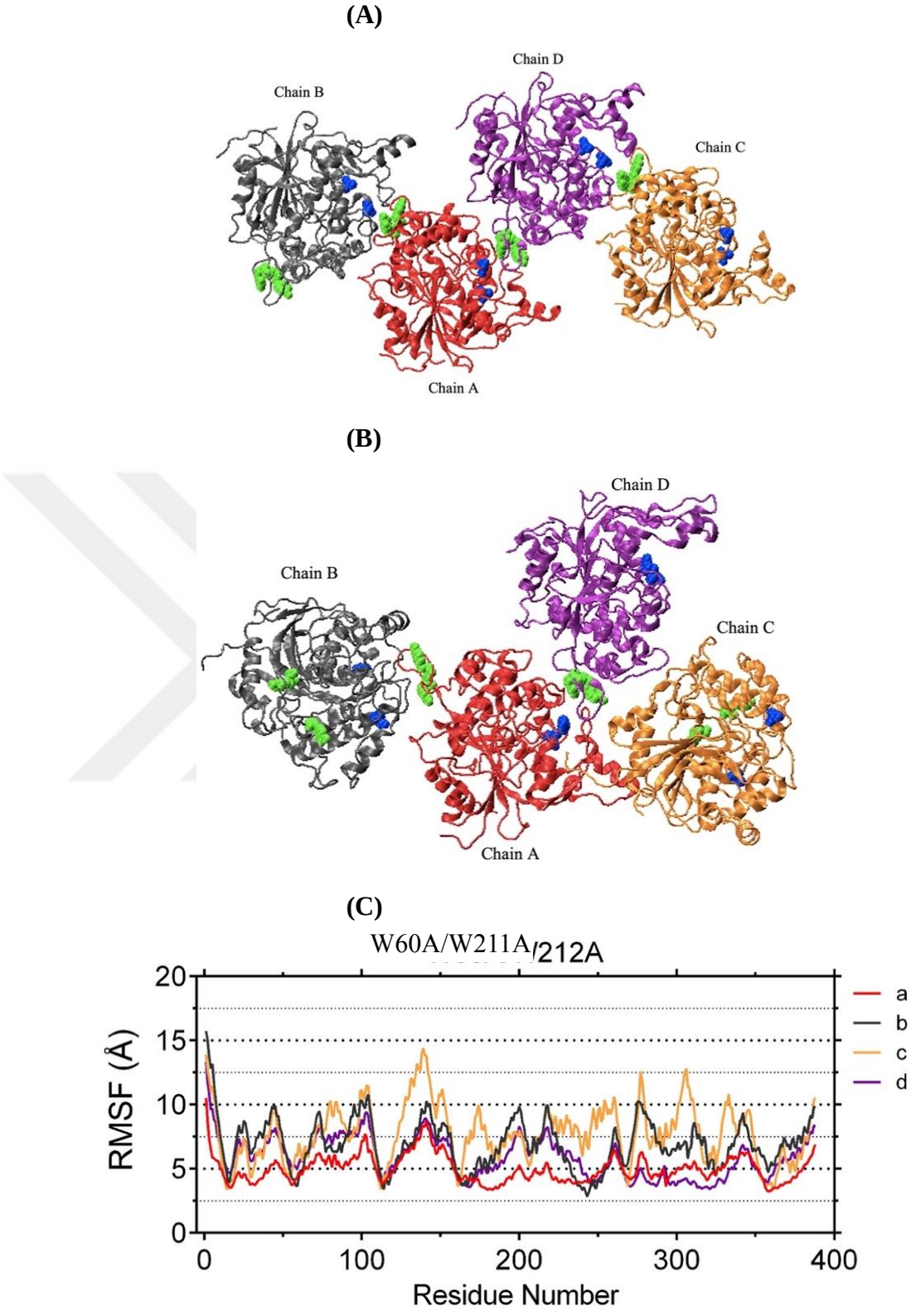

Figure 20. Root mean square fluctuation (RMSF) analysis of W60A/W211A (C). Visualization of the octamer crystal structure of before (A) and after (B) simulation by using VMD. Chains are indicated in different colors and listed in A and B. W211 region is represented with blue color, Y273 and Y282 regions are represented with green.

In Figure 20, W211/W60 tetramer mutant was analyzed and disruption was observed there as well. Looking at the RMSF result (in Figure 20C), the effect of the W211A mutation in the binding region has shown a harsher result than single W211A mutation. The outer C chain exhibited the highest mobility. The results are also supported by the laboratory experiments. Thermostability of W211A/W60A mutant decreased in the experiment and graphic showed in the Figure 24. Since it could not protect oligomeric form like the W211A mutant, it could not store its thermostability.

When Y273A/Y282A/W211A mutant was analyzed, it was understood that all chains were simulated without disruption. W211A mutation did not have the same effect on BTL2 oligomerization in this cluster. BTL2 is an aggregating enzyme. This stack structure interactions are protected in soluble state. The wild type of tetramer enzyme, in Figure 17, shows this conservation. Therefore, the non-aggregated enzyme loses its thermostability. It is clear that Y273A/Y282A/W211A mutations restore the effect of lost interactions. When the trajectory was examined, no disrupting was observed in any of the chains. Looking at the Figure 21C RMSF result, it seems that the chains remain more stable. The outer B and C chains showed more mobility, while the inner A and D chains remained more stable. No chain separation was observed in Figures 21A and 21B. This result confirms each other when compared with laboratory experiments.

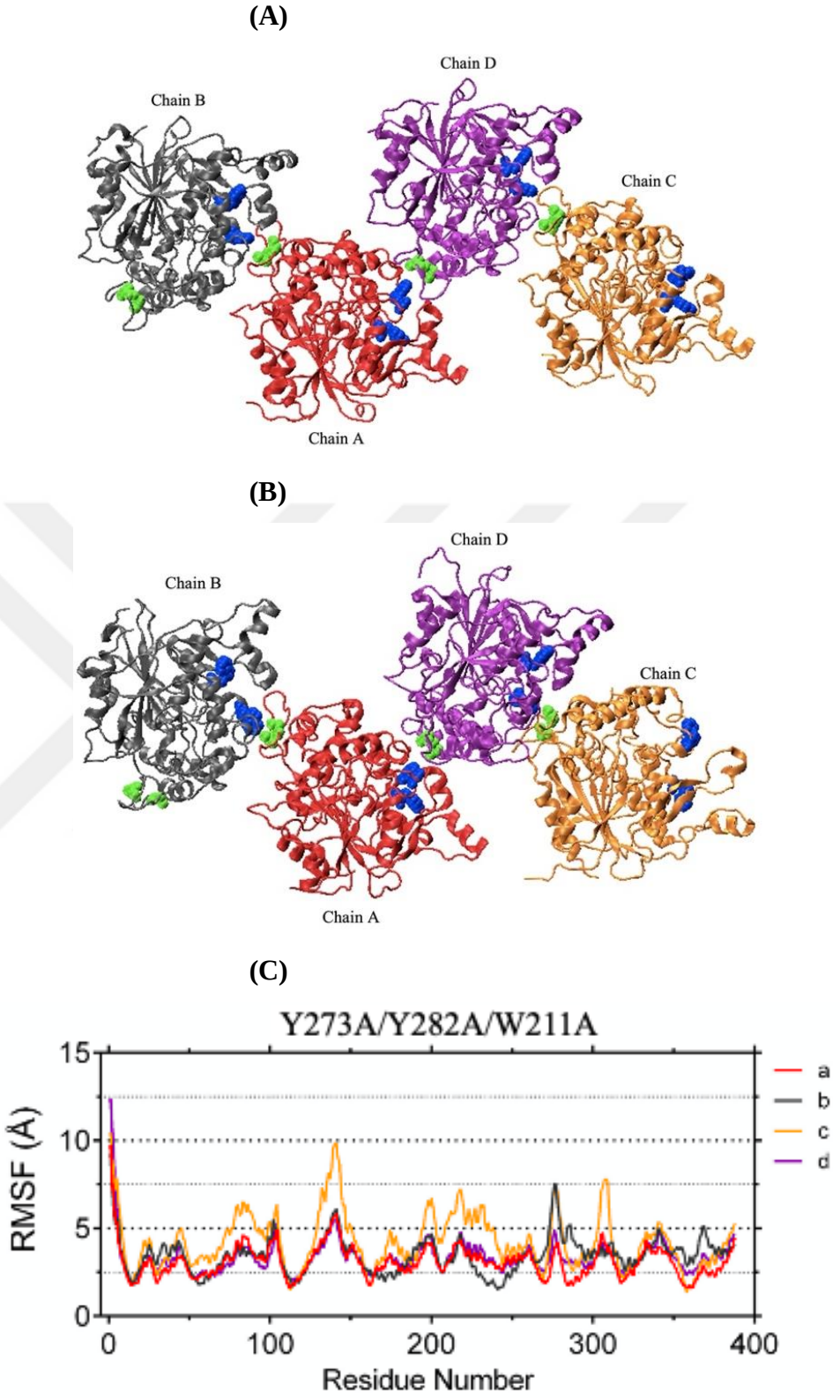

Figure 21. Root mean square fluctuation (RMSF) analysis of Y273A/Y282A/W211 mutant (C). Visualization of the octamer crystal structure of before (A) and after (B) simulation by using VMD. Chains are indicated in different colors and listed in A and B. W211 region is represented with blue color, Y273 and Y282 regions are represented with green color.

4.2 Experimental Methods

4.2.1 Lipase production

Mutated DNA samples and wild type enzyme (W60A, W211A, W60A/W211A, Y73A, Y282A, Y73A/Y282A and Y73A/Y282A/W211A) were transformed into BL21 (DE3) *E. coli* cells. Transformation results with these plasmids are shown in Figure 22. BL21 multiple colonies appeared on the plates. As seen on the plate, colonies grew sufficiently and were collected for expression.

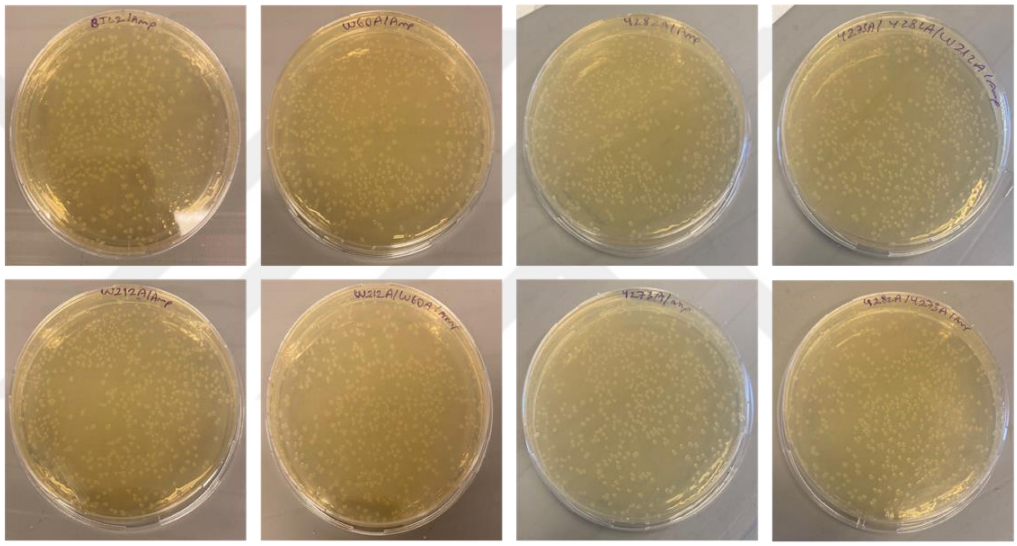

Figure 22. BL21 Transformation. BTL2 wild type, W60A, W211A, W60A/W211A, Y73A, Y282A, Y73A/Y282A and Y73A/Y282A/W211A mutation clones were transformed to BL21 cells on LB Agar ampicillin plates.

BTL2 and mutated enzymes expressed by IPTG induction, were loaded onto 10% SDS-PAGE gel after purification, at a concentration of 3 ng/ml. The gel is shown in the Figure 23. A picture showing the size of a marker is also placed next to the gel. The size of the BTL2 protein is 43 kDa, and when we look at the marker sizes on the gel, it appears to be in the 35-55 kDa range. Purified enzymes are appearing as 43 kDa. This concluded that the enzymes produced in the expected size.

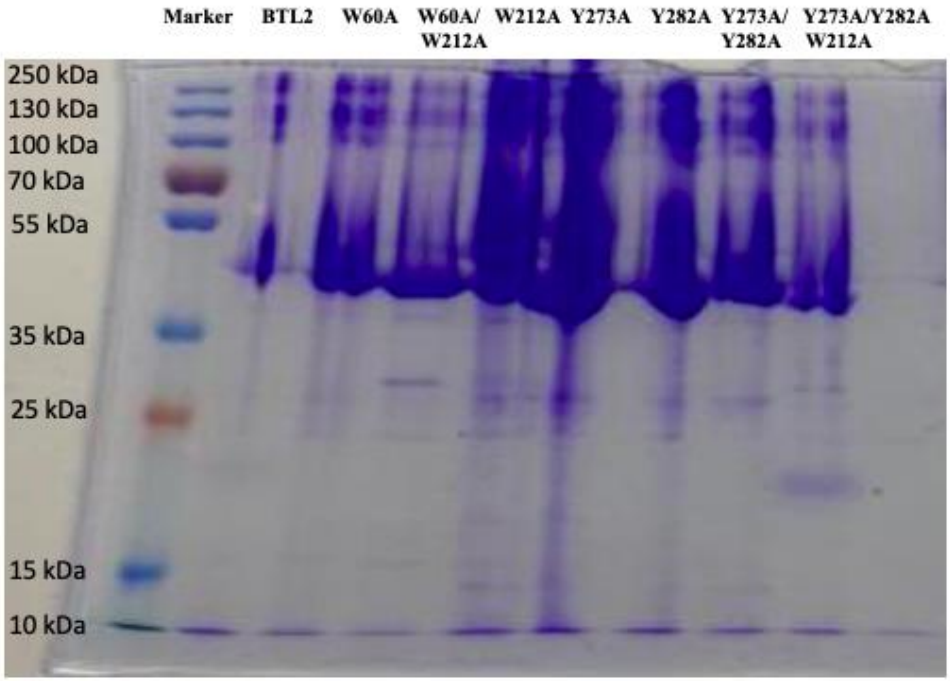

Figure 23. E. coli Shuffle Expressions. Whole cell-fraction were used from wild-type and mutants, collected after 3 hours IPTG induction. Analyzed in 10% SDS-PAGE which is stained with Coomassie blue.

In the Table 5, the concentrations are indicated in µM. W60A, W211A, W60A/W211A, Y73A, Y282A, Y73A/Y282A and Y73A/Y282A/W211A concentration measurements of purified and concentrated enzymes with Nanodrop are given. Enzyme concentrations are sufficient for the enzyme kinetic assay. Since the lowest enzyme concentration was obtained in the W60A mutant as 21 µM, highest concentration was set to 20 µM for the activity test.

Table 5. Protein concentrations measured by nanodrop (A280) are referred in μM.

Enzyme Concentrations	
Wild-type BTL2	**62 μM**
W211A	**22 μM**
W60A	**21 μM**
W60A/W211A	**24 μM**
Y273A	**140 μM**
Y282A	**266 μM**
Y273A/Y282A	**95 μM**
Y273A/Y282A/W211A	**238 μM**

4.2.2 Lipase thermostability and activity analysis

Thermostability and fluorescent assays were performed for all lipases with 250 μM 4MU-caprylate and the results are shown on the linear graph in the Figure 24. Temperatures are shown on the graph on the x axis. Thermostability experiments were carried out between 4-75 °C and tested at enzyme concentrations of 20 μM and 1 μM. Enzymes for the lipase activity assay were incubated in high and low concentrations at different temperatures.

Enzymes were diluted to a concentration of 1nM before combining with the substrate and performing the fluorescence assay. In the meantime, it was expected that all assays would be applied on an equal amount of enzyme. However, it was seen in the graphs in Figure 24 obtained that the enzymes, they did not start from the same point. This leads to the idea that enzymes could not adjusted at exactly the same concentration.

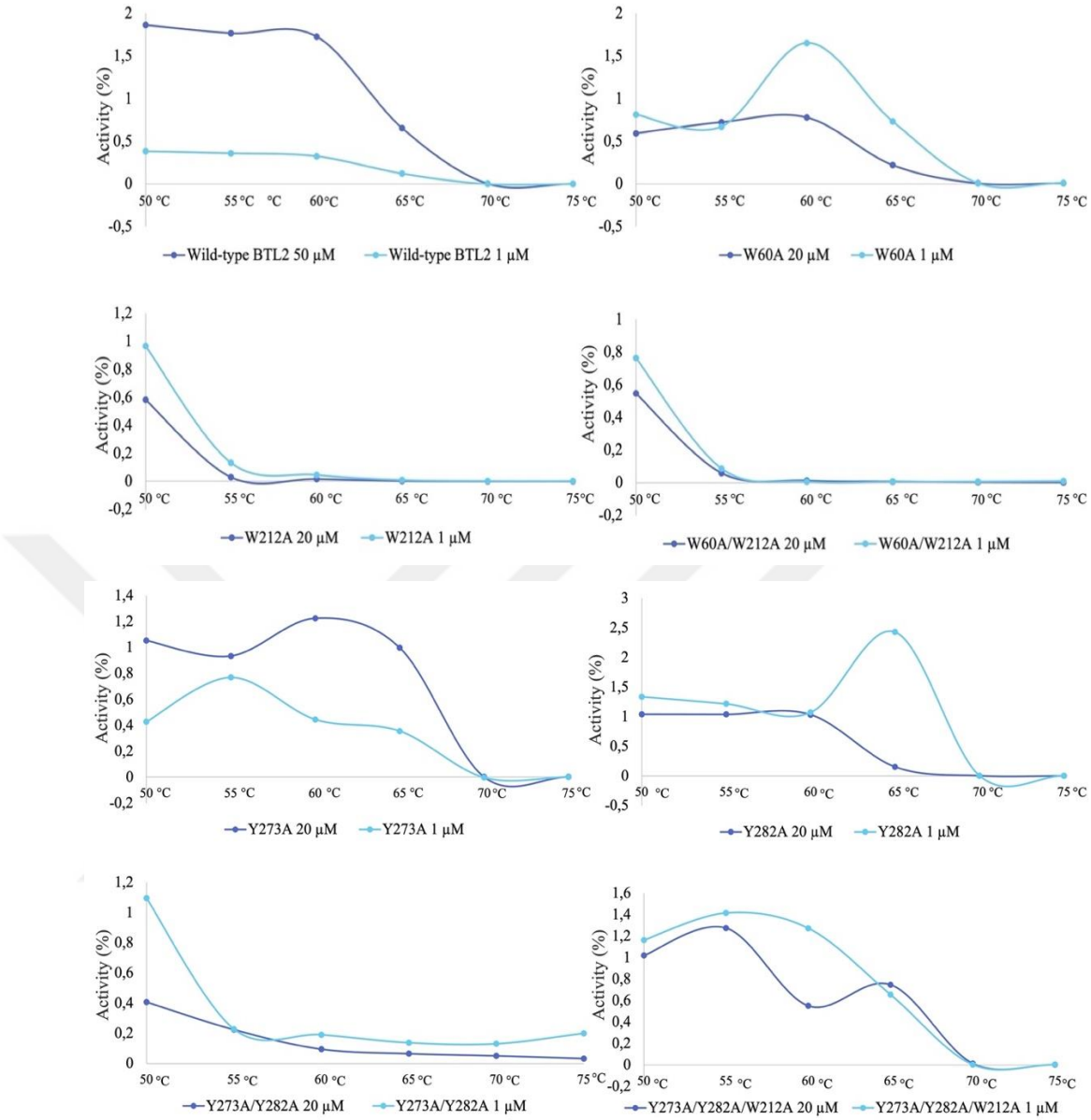

Figure 24. Residual activity versus temperature analysis. Relative fluorescent unit values were converted to percent activity by setting the activity at 4°C to 100%.

In the Figure 24, wild type BTL2 stored its activity stable up to 60°C. At higher concentration, it gave higher activity up to this temperature. After 60°C, enzyme activity decreased rapidly at both concentrations and disappeared at 70°C. Enzyme activity was measured up to 70°C, and as it can be seen from the graph, the activity is better protected at high concentrations. This means that at a high concentration, the enzyme maintains its thermostability better and can show higher activity than at a low concentration. BTL2, which is a high aggregate (14), shows higher activity at high

concentration than at low concentration, depending on the temperature. It appears that, the different concentrations do not change the degree of heat that the enzyme can tolerate, but it affects the activity.

For the W60A mutant, the high and low concentration show almost the same profile. The activity seems similar to BTL2 despite to the rate of loss of activity at high temperatures. However, unlike BTL2, the stabilization effect due to high concentration was lost. Enzyme activity at both concentrations, started to decrease after 60°C and did not show activity after 70°C. It is a region at the W211 binding interface on the lid (81) and is one of the most important mutations in this study. It also has an important role in hydrophobic interactions at the binding site. Looking at the W211A mutant in the Figure 24, the enzyme activity showed almost the same profile at high and low concentration for all temperatures. Enzyme activity started to decrease rapidly from 50°C and the activity lost at 55°C. When W211A and wild type BTL2 were compared, it was observed that W211 is at the binding interface, loss of the hydrophobic residue Trp amino acid within affected aggregation, and thermostability was lost due to this effect. The W211A/W60A double mutant showed an almost identical even more harsh profile as W211A in activity. A serious decrease is observed between 50°C -55°C in both concentrations. After 55°C, the activity is almost completely lost. This is due to disruption of hydrophobic interactions caused by mutation of W211 at the binding interface. W60A could not continue to provide that interaction here and the thermostability of the enzyme decreased. According to these results, it can be said that the W211 mutant loses its activity after 55°C.

The Y273A/Y282A mutant is on the beta sheet and has an important position in terms of the catalytic site. There was a rapid decrease in activity at high and low concentrations between 50°C - 55°C. The activity was lost at 70°C. Enzyme activity was observed to be lower in this mutant compared to the others. The Y273A mutation exhibits a very similar profile to wild type BTL2 in temperature consequences. Enzyme activity has begun to decrease after 60°C in both concentrations, and at 70°C the enzyme lost activity. Also, enzymes at high and low concentrations showed similar activity. In this respect, it can be thought that aggregation was affected by mutation.

In the Y282 mutant, he enzyme activity was affected by concentration. Enzyme activity has begun to decrease after 60°C in both concentrations, and at 70°C the enzyme no longer shows activity. The enzyme activity is lower compared to Y273, and the loss of activity was at 65°C. Interactions at the site of this mutation may have a stronger effect compared to Y273. It appears that the activity in the Y273A/Y282A/W211A mutant is generally inversely proportional to temperature at both high and low concentration as Y273A and Y282A. Enzyme activity begin to decrease after 60°C in both concentrations, and at 70°C the enzyme lost the activity. Like all other mutants, no concentration-dependent effect difference in thermostability was observed. In this mutant, the effect of disrupting thermostability in other mutants containing the W211A mutation does not appear. All the maximum temperature that enzymes gave activity is listed in Table 6.

Table 6. In the results obtained after lipase thermostability and activity analysis, the temperature ranges in which the enzyme shows the highest activity are listed.

	Temperatures	
Enzyme	**High Concentration**	**Low Concentration**
Wild-type BTL2	60°C	60°C
W211A	50°C	50°C
W60A	60°C	60°C
W60A/W211A	50°C	50°C
Y273A	60°C	55°C
Y282A	60°C	60°C
Y273A/ Y282A	50°C	50°C
Y273A/ Y282A/W211A	55°C	55°C

5 DISCUSSION

5.1 Lipase Thermostability and Activity Analysis

Binding interfaces have been studied in previous research (43,81). It was observed that hydrophobic interactions at the interface and an aromatic cluster were effective in aggregation. In addition, mutations have been made in regions that could affect this mechanism. Tryptophan (W211) in the lid region was associated with aggregation (43). In this study, based on information obtained from the literature, mutations expected to alter aggregation and thermostability were tested experimentally. Furthermore, triple aromatic clusters (Y273, Y282, W211) were observed in the earlier investigation and indicated in the interface research (82). W211, Y273 and Y282 were an important mutant in this thesis as they may be important in aggregation by hydrophobic interaction.

When the W211A mutation was introduced, the enzyme severely lost its thermostability. This is based on disruption of hydrophobic interactions caused by mutation of W211 at the binding interface. The information obtained from the literature research was in this direction and this has been confirmed in this study (43). At high concentrations, wild type BTL2 maintains its thermostability and can exhibit stronger activity than at low concentrations. This supports the idea of a thermostability preserving effect due to oligomerization.

While observing significant effects of the W211A mutant, it was expected that a loss of thermostability would also be observed in the Y273A/Y282A/W211A mutant at the beginning of the experiment. However, an interesting result was obtained from this experiment. The loss of thermostability demonstrated by the W211 mutation was not seen on Y273A/Y282A/W211A. This was an unreasonable result because the loss of W211 disrupted the hydrophobic interaction equilibrium and prevented aggregation formation. Experiments were repeated 3 times and expression was repeated 2 times to be sure. This triple mutation was observed to restore activity in all experimental trials.

It has been thought that the effect may be due to the combination of three alanine amino acids, and it may protect the structure (83).

5.2 Analyses of Molecular Dynamic Simulations

MD simulations were performed to complement the results obtained from the experiment. Aggregation consists of lipase chains assembly, like holding hands in hydrophobic cluster. Thus, the chains in the interior remain more stable. This supports our idea at the beginning of the thesis. With the effect of aggregation/oligomerization, the enzyme is protected by strong bonds and can store its thermostability.

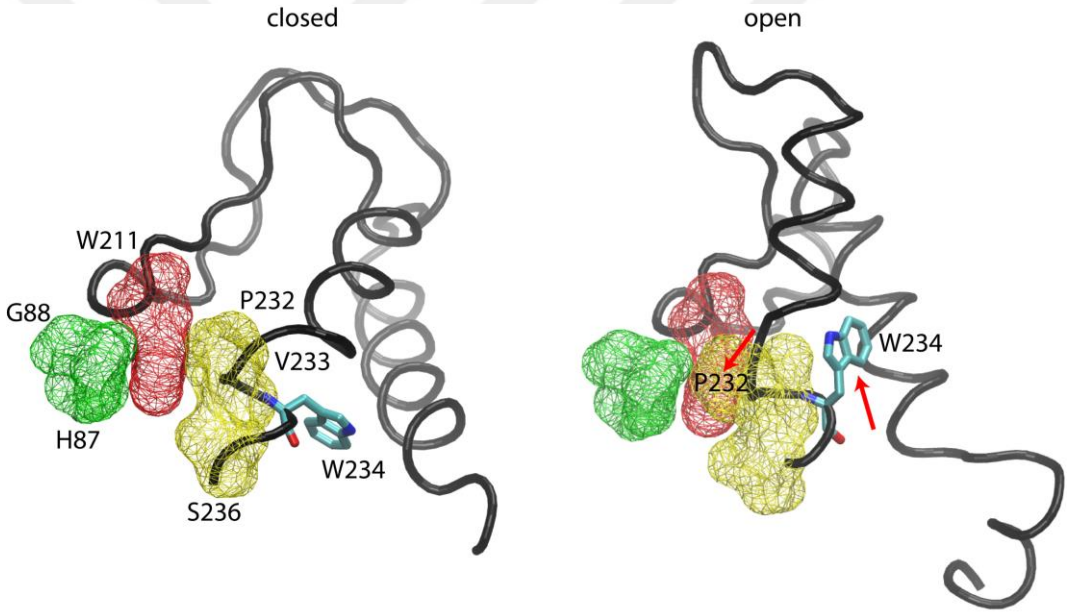

Figure 25. In the closed and open structure of BTL2, W211 in the lid region and its surroundings are shown.

Neurodegenerative diseases such as Alzheimer's and Parkinson's that affect millions of people worldwide. Generally, patients get worse over time and there is no cure for these diseases (84). Protein aggregation plays an important role in disease pathogenesis by interrupting normal cellular processes, generating toxicity, and ultimately leading to neurodegeneration (85). Understanding the mechanisms behind protein aggregation in neurodegenerative disorders are critical for creating the cure or therapy to reduce the severity of the disease's impact on patients' lives. In this thesis,

oligomer systems were created to understand the aggregation mechanism. Simulation of dimer tetramer and octamer BTL2 structures was performed in this study and contributed to the understanding of aggregation formation. It was understood that when the size of the oligomer system increase, structures show more stable feature. Because BTL2 is an ordered aggregate (82), thermo-switch can be created when hydrophobic interactions between proteins are temperature-tunable. Interactions can be set up to activate when the temperature increases to regain the activity. The development of this mechanism is vital in the development of drugs for the treatment of neurodegenerative diseases and the use of aggregated proteins in industrial production.

Since the W212 region is in the hydrophobic region, it does not want to be outside. It interacts with its surroundings in a water containing environment. As seen in Figure 25, W211 is in the open form in closed structure. In the open structure, W211 is closed by the surrounding residues. This means that, in a closed structure W211 leads to oligomerization to interact. When BTL2 is aggregated, the open part of the closed W211 region binds from the Y273 and Y282 regions of another chain. This binding region was shown in this thesis. Tetramer and octamer structure models were created from the dimer and it was shown that the W211 region is related to oligomerization using the Y273 and Y282 regions.

For the mutant systems, it was understood that the W211A mutant tetramer was disassociated. In experiments conducted in the laboratory, it was observed that thermostability was decreased in the W211A mutant. This supports the idea that W211 is on the binding interface and important for aggregation. Because of W211 is on crystal contact and aggregation interface. It directly affects thermostability and activity. On the other hand, double mutation W60A/W211A in this cluster, disrupt the formation of aggregation, thus decreasing the thermostability. It is understood that loss of tryptophan 211 in the lid, prevents the formation of oligomerization/aggregation.

While experiments of the Y273A/Y282A/W211A mutant gave unexpected result despite repeated attempts in the laboratory, it was an important analysis to examine

the state of the protein by MD simulation. This is a counter-intuitive result that removing the aromatic side-chains Y272 and Y282 restores the loss of thermostability caused by W211A. It really recovers the activity that was lost in W211A or some form of artifact a chance occurrence. However, when the three residue is mutated to alanine (W211A/Y273A/Y282A) at cluster, the thermostability protection effect of oligomerization formation was restored. These lipases have not been studied before, and the idea arose in this thesis through both experimental and computational analysis. Restoring the activity is an interesting result but needs further especially computational analysis, because just one simulation was done for triple mutation. In experimental, we see the same result but it may need re-sequencing to confirm this three-mutation position that were mutated.

Instead of Tyr and Trp interaction in activity recovery, triple alanine interaction in the cluster may have restored the activity. Jahn et al. observed activity in the protein of the polar Glu amino acid to hydrophobic Ala mutation. (86). In this study, Ala mutation, which is also hydrophobic amino acid, was made from hydrophobic Tyr and Trp amino acids. Although the situation may seem different, aromatic ring change may be affecting it (87). Also, despite the disappearance of the strong hydrophobic interactions, other interactions may have arisen and enhanced the binding for oligomerization. All of these can be explored in detail in another study in the future.

6 CONCLUSION

In conclusion, it was observed in this thesis that, the thermostability of the BTL2 enzyme resulted from oligomerization and that oligomerization occurred through a certain interface. Although aggregation causes neurodegenerative diseases in medicine, it also makes difficult to use proteins in the industrial process. Understanding the aggregation mechanism is important for the occurrence and treatment of neurodegenerative diseases. We found a model for aggregation in this study. Novel findings obtained by establishing tetramer and octamer systems on the dimer model in this thesis. When the oligomeric structures were analyzed, we found that aggregation was due to a binding interface. In all systems, the chains in the oligomer were linked to each other at the W211, Y273 and Y282 regions. Also, we noticed that the aggregation was ordered and merged as holding hands. There is information in the literature about ordered aggregation and we have confirmed it with our study. In thermostability experiments, wild type BTL2 showed a thermostable effect depending on the concentration. When the importance of hydrophobic interactions at the binding site was investigated, mutation at W211 residue cause loosing of thermostability due to affecting oligomerization. Contrary to that, no loss of thermostability was observed in the Y273A/Y282A/W211A mutant. When the computational studies were analyzed, it was seen that they supported the experimental results. This phenomenon in fact which is a counter-intuitive observation implying that deletion of Y272 and Y282 aromatic side-chains causes a restoration of the thermostability loss caused by W211A. This result needs further investigation. It really restores the activity that lost in W211A or some type of artifact an occurrence by chance. Mutations in the cluster resulted in the disintegration of the structure, except for the triple mutant. In future studies, all these simulations can be studied with metal, and the effect of metal on thermostability can be investigated.

7 REFERENCES

1. Alvizo O, Allen BD, Mayo SL. Computational protein design promises to revolutionize protein engineering. BioTechniques. 2007 Jan;42(1):31–9.

2. Sheldon RA, Woodley JM. Role of Biocatalysis in Sustainable Chemistry. Chem Rev. 2018 Jan 24;118(2):801–38.

3. Godoy CA, Klett J, Di Geronimo B, Hermoso JA, Guisán JM, Carrasco-López C. Disulfide Engineered Lipase to Enhance the Catalytic Activity: A Structure-Based Approach on BTL2. Int J Mol Sci. 2019 Oct 23;20(21):5245.

4. Kapoor S, Rafiq A, Sharma S. Protein engineering and its applications in food industry. Crit Rev Food Sci Nutr. 2017 Jul 24;57(11):2321–9.

5. Liu Q, Xun G, Feng Y. The state-of-the-art strategies of protein engineering for enzyme stabilization. Biotechnol Adv. 2019 Jul;37(4):530–7.

6. Rubingh DN, Grayling RA. Protein Engineering. Protein Eng.

7. Ordu E, Gul N. Protein Engineering Applications on Industrially Important Enzymes: Candida methylica FDH as a Case Study. In: Kaumaya P, editor. Protein Engineering [Internet]. InTech; 2012 [cited 2023 Jun 25]. Available from: http://www.intechopen.com/books/protein-engineering/protein-engineering-applications-on-industrially-important-enzymes-candida-methylica-fdh-as-a-case-s

8. Wunderlich M, Martin A, Staab CA, Schmid FX. Evolutionary Protein Stabilization in Comparison with Computational Design. J Mol Biol. 2005 Sep;351(5):1160–8.

9. Karplus M, McCammon JA. Molecular dynamics simulations of biomolecules. Nat Struct Biol. 2002;9(9).

10. Phillips JC, Braun R, Wang W, Gumbart J, Tajkhorshid E, Villa E, et al. Scalable molecular dynamics with NAMD. J Comput Chem. 2005 Dec;26(16):1781–802.

11. Brooks BR, Brooks CL, Mackerell AD, Nilsson L, Petrella RJ, Roux B, et al. CHARMM: The biomolecular simulation program. J Comput Chem. 2009 Jul 30;30(10):1545–614.

12. Weiner SJ, Kollman PA, Nguyen DT, Case DA. An all atom force field for simulations of proteins and nucleic acids: An All Atom Force Field. J Comput Chem. 1986 Apr;7(2):230–52.

13. CHARMM-GUI [Internet]. [cited 2023 Jun 25]. Available from: https://www.charmm-gui.org/?doc=about

14. Yenenler A, Venturini A, Burduroglu HC, Sezerman OU. Investigating the structural properties of the active conformation BTL2 of a lipase from Geobacillus thermocatenulatus in toluene using molecular dynamic simulations and engineering BTL2 via in-silico mutation. J Mol Model. 2018 Sep;24(9):229.

15. Jaeger KE, Dijkstra BW, Reetz MT. Bacterial Biocatalysts: Molecular Biology, Three-Dimensional Structures, and Biotechnological Applications of Lipases. Annu Rev Microbiol. 1999 Oct;53(1):315–51.

16. Ribeiro BD, Castro AMD, Coelho MAZ, Freire DMG. Production and Use of Lipases in Bioenergy: A Review from the Feedstocks to Biodiesel Production. Enzyme Res. 2011 Jul 7;2011:1–16.

17. Dodson GG, Lawson DM, Winkler FK. Structural and evolutionary relationships in lipase mechanism and activation. Faraday Discuss. 1992;93:95.
18. Vaysse L, Ly A, Moulin G, Dubreucq E. Chain-length selectivity of various lipases during hydrolysis, esterification and alcoholysis in biphasic aqueous medium. Enzyme Microb Technol. 2002 Oct;31(5):648–55.
19. Ema T. Rational strategies for highly enantioselective lipase-catalyzed kinetic resolutions of very bulky chiral compounds: substrate design and high-temperature biocatalysis. Tetrahedron Asymmetry. 2004 Sep;15(18):2765–70.
20. Hari Krishna S, Manohar B, Divakar S, Prapulla SG, Karanth NG. Optimization of isoamyl acetate production by using immobilized lipase from Mucor miehei by response surface methodology. Enzyme Microb Technol. 2000 Feb;26(2–4):131–6.
21. Peters GH, Van Aalten DM, Svendsen A, Bywater R. Essential dynamics of lipase binding sites: the effect of inhibitors of different chain length. Protein Eng Des Sel. 1997 Feb 1;10(2):149–58.
22. Secundo F, Carrea G, Tarabiono C, Gatti-Lafranconi P, Brocca S, Lotti M, et al. The lid is a structural and functional determinant of lipase activity and selectivity. J Mol Catal B Enzym. 2006 May;39(1–4):166–70.
23. Park JY, Park KM. Lipase and Its Unique Selectivity: A Mini-Review. Haque A, editor. J Chem. 2022 Oct 8;2022:1–11.
24. Brady L, Brzozowski AM, Derewenda ZS, Dodson E, Dodson G, Tolley S, et al. A serine protease triad forms the catalytic centre of a triacylglycerol lipase. Nature. 1990 Feb;343(6260):767–70.
25. Carrasco-López C, Godoy C, De Las Rivas B, Fernández-Lorente G, Palomo JM, Guisán JM, et al. Activation of Bacterial Thermoalkalophilic Lipases Is Spurred by Dramatic Structural Rearrangements. J Biol Chem. 2009 Feb;284(7):4365–72.
26. Kapoor M, Gupta MN. Lipase promiscuity and its biochemical applications. Process Biochem. 2012 Apr;47(4):555–69.
27. Wong H, Schotz MC. The lipase gene family. J Lipid Res. 2002 Jul;43(7):993–9.
28. Muralidhar RV, Chirumamilla RR, Marchant R, Ramachandran VN, Ward OP, Nigam P. Understanding lipase stereoselectivity.
29. Aucoin MG, Erhardt FA, Legge RL. Hyperactivation ofRhizomucor miehei lipase by hydrophobic xerogels. Biotechnol Bioeng. 2004 Mar 20;85(6):647–55.
30. Rahman MZA, Salleh AB, Rahman RNZRA, Rahman MBA, Basri M, Leow TC. Unlocking the mystery behind the activation phenomenon of T1 lipase: A molecular dynamics simulations approach. Protein Sci. 2012 Aug;21(8):1210–21.
31. Petrella RJ, Karplus M. The role of carbon-donor hydrogen bonds in stabilizing tryptophan conformations: Carbon Donor Hydrogen Bonds. Proteins Struct Funct Bioinforma. 2004 Mar 1;54(4):716–26.
32. Bank RPD. RCSB PDB - 1JI3: CRYSTAL STRUCTURE OF THE FIRST THERMOSTABLE BACTERIAL LIPASE FROM BACILLUS STEAROTHERMOPHILUS [Internet]. [cited 2023 Jun 30]. Available from: https://www.rcsb.org/structure/1JI3

33. Chandra P, Enespa, Singh R, Arora PK. Microbial lipases and their industrial applications: a comprehensive review. Microb Cell Factories. 2020 Dec;19(1):169.
34. Gutiérrez A. The biotechnological control of pitch in paper pulp manufacturing. Trends Biotechnol. 2001 Sep 1;19(9):340–8.
35. Piamtongkam R, Duquesne S, Bordes F, Barbe S, André I, Marty A, et al. Enantioselectivity of Candida rugosa lipases (Lip1, Lip3, and Lip4) towards 2-bromo phenylacetic acid octyl esters controlled by a single amino acid. Biotechnol Bioeng. 2011 Aug;108(8):1749–56.
36. Haki G. Developments in industrially important thermostable enzymes: a review. Bioresour Technol. 2003 Aug;89(1):17–34.
37. Arpigny JL, Jaeger KE. Bacterial lipolytic enzymes : classification and properties. 1999;
38. Fernandez-Lorente G, Godoy CA, Mendes AA, Lopez-Gallego F, Grazu V, De Las Rivas B, et al. Solid-Phase Chemical Amination of a Lipase from Bacillus thermocatenulatus To Improve Its Stabilization via Covalent Immobilization on Highly Activated Glyoxyl-Agarose. Biomacromolecules. 2008 Sep 8;9(9):2553–61.
39. Schmidt-Dannert C, Luisa Rúa M, Schmid RD. [11] Two novel lipases from thermophile Bacillus thermocatenulatus: Screening, purification, cloning, overexpression, and properties. In: Methods in Enzymology [Internet]. Elsevier; 1997 [cited 2023 Jul 1]. p. 194–220. Available from: https://linkinghub.elsevier.com/retrieve/pii/S007668799784013X
40. Quyen DT, Schmidt-Dannert C, Schmid RD. High-level expression of a lipase from Bacillus thermocatenulatus BTL2 in Pichia pastoris and some properties of the recombinant lipase. Protein Expr Purif. 2003 Mar;28(1):102–10.
41. Schmidt-Dannert C, Sztajer H, Stöcklein W, Menge U, Schmid RD. Screening, purification and properties of a thermophilic lipase from Bacillus thermocatenulatus. Biochim Biophys Acta BBA - Lipids Lipid Metab. 1994 Aug;1214(1):43–53.
42. Align | UniProt [Internet]. [cited 2023 Jul 4]. Available from: https://www.uniprot.org/align
43. Timucin E, Sezerman OU. The Conserved Lid Tryptophan, W211, Potentiates Thermostability and Thermoactivity in Bacterial Thermoalkalophilic Lipases. Colombo G, editor. PLoS ONE. 2013 Dec 31;8(12):e85186.
44. Ollis DL, Cheah E, Cygler M, Dijkstra B, Frolow F, Franken SM, et al. The α / β hydrolase fold. Protein Eng Des Sel. 1992;5(3):197–211.
45. Jeong ST, Kim HK, Kim SJ, Chi SW, Pan JG, Oh TK, et al. Novel Zinc-binding Center and a Temperature Switch in theBacillus stearothermophilus L1 Lipase. J Biol Chem. 2002 May;277(19):17041–7.
46. Hung CW, Chen YC, Hsieh WL, Chiou SH, Kao CL. Ageing and neurodegenerative diseases. Ageing Res Rev. 2010 Nov;9:S36–46.
47. Ross CA, Poirier MA. Protein aggregation and neurodegenerative disease. Nat Med. 2004 Jul;10(S7):S10–7.
48. Hansson O. Biomarkers for neurodegenerative diseases. Nat Med. 2021 Jun;27(6):954–63.

49. Schlieben NH, Niefind K, Schomburg D. Expression, purification, and aggregation studies of His-tagged thermoalkalophilic lipase from Bacillus thermocatenulatus. Protein Expr Purif. 2004 Mar;34(1):103–10.
50. Rúa ML, Schmidt-Dannert C, Wahl S, Sprauer A, Schmid RD. Thermoalkalophilic lipase of Bacillus thermocatenulatus large-scale production, purification and properties: aggregation behaviour and its effect on activity. J Biotechnol. 1997 Aug 11;56(2):89–102.
51. D[illegible]nhaupt A, Lang S, Wagner F. Pseudomonas cepacia lipase: Studies on aggregation, purification and on the cleavage of olive oil. Biotechnol Lett. 1992 Oct;14(10):953–8.
52. Rabindran SK, Haroun RI, Clos J, Wisniewski J, Wu C. Regulation of Heat Shock Factor Trimer Formation: Role of a Conserved Leucine Zipper. Science. 1993 Jan 8;259(5092):230–4.
53. Peters GH, Olsen OH, Svendsen A, Wade RC. Theoretical investigation of the dynamics of the active site lid in Rhizomucor miehei lipase. Biophys J. 1996 Jul;71(1):119–29.
54. Zhu K, Jutila A, Tuominen EKJ, Patkar SA, Svendsen A, Kinnunen PKJ. Impact of the tryptophan residues of Humicola lanuginosa lipase on its thermal stability. Biochim Biophys Acta BBA - Protein Struct Mol Enzymol. 2001 Jun;1547(2):329–38.
55. Kazlauskas RJ, Bornscheuer UT. Finding better protein engineering strategies. Nat Chem Biol. 2009 Aug;5(8):526–9.
56. Chado GR, Holland EN, Tice AK, Stoykovich MP, Kaar JL. Modification of Lipase with Poly(4-acryloylmorpholine) Enhances Solubility and Transesterification Activity in Anhydrous Ionic Liquids. Biomacromolecules. 2018 Apr 9;19(4):1324–32.
57. Ventura S. Sequence determinants of protein aggregation: tools to increase protein solubility. Microb Cell Factories. 2005 Dec;4(1):11.
58. Chihara-Siomi M, Yoshikawa K, Oshima-Hirayama N, Yamamoto K, Sogabe Y, Nakatani T, et al. Purification, molecular cloning, and expression of lipase from Pseudomonas aeruginosa. Arch Biochem Biophys. 1992 Aug;296(2):505–13.
59. Jaeger KE, Eggert T. Lipases for biotechnology. Curr Opin Biotechnol. 2002 Aug;13(4):390–7.
60. Houde A, Kademi A, Leblanc D. Lipases and Their Industrial Applications: An Overview. Appl Biochem Biotechnol. 2004;118(1–3):155–70.
61. Bornscheuer UT, Huisman GW, Kazlauskas RJ, Lutz S, Moore JC, Robins K. Engineering the third wave of biocatalysis. Nature. 2012 May;485(7397):185–94.
62. UCSF Chimera Home Page [Internet]. [cited 2023 Jul 1]. Available from: https://www.cgl.ucsf.edu/chimera/
63. Vanommeslaeghe K, Hatcher E, Acharya C, Kundu S, Zhong S, Shim J, et al. CHARMM general force field: A force field for drug-like molecules compatible with the CHARMM all-atom additive biological force fields. J Comput Chem. 2009;NA-NA.
64. Izaguirre JA, Catarello DP, Wozniak JM, Skeel RD. Langevin stabilization of molecular dynamics. J Chem Phys. 2001 Feb;114(5):2090–8.
65. VMD - Visual Molecular Dynamics [Internet]. [cited 2023 Jul 1]. Available from: https://www.ks.uiuc.edu/Research/vmd/

66. Sargsyan K, Grauffel C, Lim C. How Molecular Size Impacts RMSD Applications in Molecular Dynamics Simulations. J Chem Theory Comput. 2017 Apr 11;13(4):1518–24.
67. Srikumar PS, Rohini K, Rajesh PK. Molecular Dynamics Simulations and Principal Component Analysis on Human Laforin Mutation W32G and W32G/K87A. Protein J. 2014 Jun;33(3):289–95.
68. Nair IM, Jayachandran K. In Vitro Enzymatic Conversion of Glibenclamide Using Squalene Hopene Cyclase from Pseudomonas mendocina Expressed in E. coli BL21 (DE3). Mol Biotechnol. 2020 Sep;62(9):456–65.
69. Pulido IY, Prieto E, Pieffet GP, Méndez L, Jiménez-Junca CA. Functional Heterologous Expression of Mature Lipase LipA from Pseudomonas aeruginosa PSA01 in Escherichia coli SHuffle and BL21 (DE3): Effect of the Expression Host on Thermal Stability and Solvent Tolerance of the Enzyme Produced. Int J Mol Sci. 2020 May 30;21(11):3925.
70. Gomes L, Monteiro G, Mergulhão F. The Impact of IPTG Induction on Plasmid Stability and Heterologous Protein Expression by Escherichia coli Biofilms. Int J Mol Sci. 2020 Jan 16;21(2):576.
71. Zhang J, Tian M, Lv P, Luo W, Wang Z, Xu J, et al. High-efficiency expression of the thermophilic lipase from Geobacillus thermocatenulatus in Escherichia coli and its application in the enzymatic hydrolysis of rapeseed oil. 3 Biotech. 2020 Dec;10(12):523.
72. Falke JJ, Corbin JA. Affinity Tags for Protein Purification. In: Encyclopedia of Biological Chemistry [Internet]. Elsevier; 2013 [cited 2023 Jul 6]. p. 61–5. Available from: https://linkinghub.elsevier.com/retrieve/pii/B9780123786302001730
73. Wang F, Ren X, Chen Z, Li X, Zhu H, Li S, et al. The N- terminal His- tag affects the triglyceride lipase activity of hormone- sensitive lipase in testis. J Cell Biochem. 2019 Aug;120(8):13706–16.
74. Pirmanesh S, Kermanshahi RK, Gharavi S, Mobarak Qamsari E. Cloning, Expression, and Purification of a GDSL-like Lipase/Acylhydrolase from a Native Lipase-Producing Bacterium, Lactobacillus fermentum. Iran Biomed J. 2022 Mar;26(2):153–9.
75. Nawani N, Kaur J. Purification, characterization and thermostability of lipase from a thermophilic Bacillus sp. J33.
76. Desjardins P, Hansen JB, Allen M. Microvolume Protein Concentration Determination Using the NanoDrop 2000c Spectrophotometer. J Vis Exp. 2009 Nov 4;(33):1610.
77. Bitou N, Ninomiya M, Tsujita T, Okuda H. Screening of lipase inhibitors from marine algae. Lipids. 1999 May;34(5):441–5.
78. Hamilton BK, Gardner CR, Colton CK. Effect of diffusional limitations on lineweaver-burk plots for immobilized enzymes. AIChE J. 1974 May;20(3):503–10.
79. Ibrahim K. Normal Standard Curve for Acoustic Pharyngometry. Otolaryngol Neck Surg. 2001 Mar;124(3):323–30.
80. Hamid THAbd, Rahman RNZRAbd, Salleh AB, Basri M. The Role of Lid in Protein-Solvent Interaction of the Simulated Solvent Stable Thermostable Lipase from *Bacillus* Strain 42 in Water-Solvent Mixtures. Biotechnol Biotechnol Equip. 2009 Jan;23(4):1524–30.

81. Timucin E, Cousido-Siah A, Mitschler A, Podjarny A, Sezerman OU. Probing the roles of two tryptophans surrounding the unique zinc coordination site in lipase family I.5: Molecular Machinery of Zinc Induced Stability. Proteins Struct Funct Bioinforma. 2016 Jan;84(1):129–42.
82. Timucin E, Sezerman OU. Zinc Modulates Self-Assembly of *Bacillus thermocatenulatus* Lipase. Biochemistry. 2015 Jun 30;54(25):3901–10.
83. Qiu L, Yan Y, Sun Z, Song J, Zhang JZH. Interaction entropy for computational alanine scanning in protein–protein binding. WIREs Comput Mol Sci [Internet]. 2018 Mar [cited 2023 Jul 22];8(2). Available from: https://onlinelibrary.wiley.com/doi/10.1002/wcms.1342
84. Simonian NA. Oxidative Stress in Neurodegenerative Diseases.
85. Soto C, Pritzkow S. Protein misfolding, aggregation, and conformational strains in neurodegenerative diseases. Nat Neurosci. 2018 Oct;21(10):1332–40.
86. Jahn M, Chen H, Müllegger J, Marles J, Warren RAJ, Withers SG. Thioglycosynthases: double mutant glycosidases that serve as scaffolds for thioglycoside synthesis. Chem Commun. 2004;(3):274–5.
87. Robinson J, Snyder MA, Belisle C, Liao J li, Chen H, He X, et al. Investigating the impact of aromatic ring substitutions on selectivity for a multimodal anion exchange prototype library. J Chromatogr A. 2018 Sep;1569:101–9.

8 APPENDIX

Table 1. Binding buffer preparation.

25mM Imidazole Binding Buffer	Ingredient Amount
10X TBS	20 ml
1M Imidazole	5 ml
DDW	Up to 200 ml

Table 2. Wash buffer preparation.

40mM Imidazole Wash Buffer	Ingredient Amount
10X TBS	20 ml
1M Imidazole	8 ml
DDW	Up to 200 ml

Table 3. Elution buffer preparation.

200mM Imidazole Elution Buffer	Ingredient Amount
10X TBS	5 ml
1M Imidazole	10 ml
DDW	Up to 50 ml

Table 4. SDS-PAGE buffer for the lower gel.

SDS-PAGE gel buffer - Lower (pH 8.8)	Ingredient Amount
SDS	1.75 g
Tris	90.75 g
DDW	Up to 500 ml

Table 5. SDS-PAGE buffer for the upper gel.

SDS-PAGE gel buffer - Upper (pH 6.8)	Ingredient Amount
SDS Tris	3.7 g
Tris	60.5 g
DDW	Up to 500 ml

Table 6 Sample buffer for loading protein samples on SDS-PAGE gel. Final concentration 1X used.

SDS-PAGE Sample Buffer (3X)	Ingredient Amount
Bromophenol Blue Beta-mercaptoethanol	10 mg
Beta-mercaptoethanol	5 ml
SDS	3 g
Glycerol	10-24 ml
Upper Tris Buffer (Appendix Table 5)	6.25 ml
DDW	Up to 100 ml

Table 7. SDS-PAGE gel running buffer for gel electrophoresis.

SDS Running Buffer (10X)	Ingredient Amount
SDS	50 g 151.43 g
Tris	151.43 g
Glycine	720.7 g
DDW	Up to 5 liters

Table 8. SDS-PAGE gel stain solution (Reusable).

SDS-PAGE Gel Stain	Ingredient Amount
Methanol	500 ml 2 g
Coomassie Blue BB R-250	2 g
↓ Filter Though 3MM Filter Paper ↓	
Acetic Acid	100 ml
DDW	400 ml

Table 9. SDS-PAGE gel detain solution.

SDS-PAGE Gel Destain	Ingredient Amount
Methanol	400 ml
Acetic Acid	140 ml
DDW	1460 ml

Table 10. Lower gel preparation for polyacrylamide SDS-PAGE gel.

10% SDS Lower Gel	Ingredient Amount
DDW	6.4 ml
Acrylamide	3.3 ml
1.5M Tris pH 8.8	3.25 ml
10 percent APS	0.130 ml
TEMED	0.005 ml

Table 11. Upper gel preparation for polyacrylamide SDS-PAGE gel.

10% SDS Upper Gel	Ingredient Amount
DDW	2.5 ml
Acrylamide	0.425 ml
1.5M Tris pH 8.8	0.430 ml
10 percent APS	0.034 ml
TEMED	0.004 ml

Table 12. 200x Protease Inhibitor stock solution preparation.

Protease Inhibitor (200X)	**Ingredient Amount**
PMSF	350 mg
Benzamidine	120 mg
Benzamide	15 mg
Ethanol	Up to 10 ml

9 CURRICULUM VITAE